

William D. Lakin · Scott A. Stevens · Bruce I. Tranmer · Paul L. Penar

A whole-body mathematical model for intracranial pressure dynamics

Received: 30 October 2001 / Revised version: 15 September 2002 /
Published online: 18 December 2002 – © Springer-Verlag 2002

Abstract. Most attempts to study intracranial pressure using lumped-parameter models have adopted the classical “Kellie-Monro Doctrine,” which considers the intracranial space to be a closed system that is confined within the nearly-rigid skull, conserves mass, and has equal inflow and outflow. The present work revokes this Doctrine and develops a mathematical model for the dynamics of intracranial pressures, volumes, and flows that embeds the intracranial system in extensive whole-body physiology. The new model consistently introduces compartments representing the tissues and vasculature of the extradural portions of the body, including both the thoracic region and the lower extremities. In addition to vascular connections, a spinal-subarachnoid cerebrospinal fluid (CSF) compartment bridges intracranial and extracranial physiology allowing explicit buffering of intracranial pressure fluctuations by the spinal theca. The model contains cerebrovascular autoregulation, regulation of systemic vascular pressures by the sympathetic nervous system, regulation of CSF production in the choroid plexus, a lymphatic system, colloid osmotic pressure effects, and realistic descriptions of cardiac output. To validate the model in situations involving normal physiology, the model’s response to a realistic pulsatile cardiac output is examined. A well-known experimentally-derived intracranial pressure-volume relationship is recovered by using the model to simulate CSF infusion tests, and the effect on cerebral blood flow of a change in body position is also examined. Cardiac arrest and hemorrhagic shock are simulated to demonstrate the predictive capabilities of the model in pathological conditions.

1. Introduction

Lumped-parameter models represent an attractive method for examining pressure dynamics involving complicated human physiology. In this modeling approach, the physiological system is subdivided into a number of linked, interacting subunits termed “compartments.” In general, each compartment will contain a single physical constituent, such as blood, cerebrospinal fluid (CSF), or tissue and interstitial fluid. However, depending on the model’s complexity, a given constituent may appear in more than one compartment of the model. Dynamics in each compartment

W.D. Lakin: Department of Mathematics and Statistics, University of Vermont, 16 Colchester Avenue, Burlington, VT, 05401-1455, USA. e-mail: wlakin@together.net

S.A. Stevens: School of Science, Penn State Erie, The Behrend College, Erie, PA, 16563 USA. e-mail: sas56@psu.edu

B.I. Tranmer, P.L. Penar: Division of Neurosurgery, University of Vermont, Burlington, VT, 05405, USA. e-mail: btranmer@zoo.uvm.edu; Paul.Penar@vtmednet.org

Key words or phrases: Intracranial pressure dynamics – Lumped-parameter models – Whole body physiology – Pressure-volume relationships

is specified by lumped, time-dependent functions giving compartmental pressures, while incremental changes in flows and compartmental volumes are obtained by associating resistance and compliance parameters with adjacent compartments. In particular, interaction between adjacent subunits is assumed to take place at the interfaces of the model's compartments.

Models of this type have been used to study intracranial pressure for more than 200 years. However, with few exceptions, previous models have adopted restrictions known as the "Kellie-Monro Doctrine" to reduce complexity. The Kellie-Monro framework considers the intracranial system to be completely enclosed within the intracranial vault, which is assumed to be rigid. A specified inflow of blood to the intracranial arteries provides a forcing for the system, and outflow from the Jugular Bulb is assumed to instantaneously equate to this inflow. These restrictions yield a closed system with constant total volume. Strictly intracranial models have produced a number of important results that illuminate the mechanisms of intracranial pressure adjustments in situations involving both normal and pathophysiology. However, the ability of these closed-system models to incorporate the influence of important extracranial factors on intracranial pressure dynamics is clearly limited. For example, the important buffering effects of the spinal CSF space on intracranial pressure cannot be directly included. From a mathematical point of view, the constant-volume constraint also produces an overdetermined system of equations that requires special handling to avoid singular behavior.

The present model revokes the Kellie-Monro Doctrine by consistently embedding the intracranial system within whole-body physiology. It involves 16 interacting compartments, of which 9 lie entirely outside of the intracranial vault. Two distinct compartments are defined to distinguish ventricular from extraventricular CSF. The vasculature of the intracranial system within the cranial vault is also subdivided into five compartments representing fluid in the intracranial arteries, capillaries, choroid plexus, veins, and venous sinus. The body's extracranial systemic vasculature is divided into six compartments representing the arteries, capillaries, and veins of the central body and the lower body. Tissue and the associated interstitial fluid in the intracranial and lower regions is divided into two compartments. A composite compartment involving the tissues, organs, and pulmonary circulation of the central body and an implicit compartment representing the external environment complete the model. Since the time-dependent compartmental pressure functions are obtained from physical pressures through a "lumping" procedure that involves space-averaging over the physical extent of a compartment, the subdivision of physical constituents into distinct spatially-limited compartments is necessary to provide spatial resolution in this modeling approach.

In addition to allowing direct flows (e.g. arteries to capillaries to veins) between adjacent compartments, the present work includes the extracranial transfer of fluid between capillaries and tissue by filtration. An extracranial lymphatic system is also included in the model. Components of the model allow regulation of systemic vascular pressures by the sympathetic nervous system, and, at less than extreme (high or low) pressures, autoregulation mechanisms provide constant blood flow to the cerebrovascular capillaries and the choroid plexus as well as constant production of CSF in the choroid plexus. Fluid intake, renal output of fluid, and adjustment

of body volume in response to changes in ambient environmental pressure are allowed. A realistic representation for cardiac uptake and cardiac output provides the forcing for this system.

The form of the present model is a system of governing differential equations for the fully time-dependent compartmental pressure functions. A key component of the present work is determining appropriate forms for the non-constant resistance and compliance parameters in the model, which may be functions of both pressures and time. Calibration of physically-realistic scale values for parameters and flows is also a key step in the simulation process.

2. Methods

In the present mathematical model, the human body is divided into 16 distinct compartments, as depicted in Figure 1. To help delineate the intracranial system, the thick line in Figure 1 represents the cranial vault which differentiates intracranial from extra-cranial compartments. The “lower” compartments represent the region below the pelvis. The “central” compartments in the model represent the region between the lower body and the clavicles and also include extracranial body components above the clavicles but outside of the cranial wall. Eight compartments in Figure 1 lie completely outside of the cranial vault, and a ninth compartment includes both intracranial and extracranial physiology.

The majority of the compartments in the current model are vascular. The 11 vascular compartments can be subdivided spatially into three groups: intracranial (compartments A, C, P, V, and S), central (I, J, and O) and lower (Z, D, and X). There are 4 strictly non-vascular model subunits. These compartments represent tissue matter and interstitial fluid (lower compartment G and brain compartment B), as well as two cerebrospinal fluid compartments: Ventricular (F) and extra-ventricular (T). It should be noted that compartment T is both an intracranial and a central compartment. The rest-of-body compartment (Y) is a composite compartment consisting of the pulmonary circulation, organs, tissue matter and interstitial fluid. The external environment (compartment M) is also an implicit 17-th subunit in the model. No attempt has been made to depict relative volumes in Figure 1, and hence the relative sizes of these compartments in the figure do not reflect relative volumes.

The pressure dynamics of the lumped-parameter model are described by a system of differential equations derived below in section 2.1. Prior to solving these equations, it is necessary to determine appropriate forms and approximate scale values for various model parameters. These parameters are calibrated in section 2.2. Furthermore, the model contains cardiac forcing and autoregulatory mechanisms for cardiac uptake, arterial pressure, intracranial blood supply, CSF production, and lymphatic flow. These are described in section 2.3

2.1. Derivation of the governing equations

Four basic assumptions lead to the equations describing the pressure dynamics of this system:

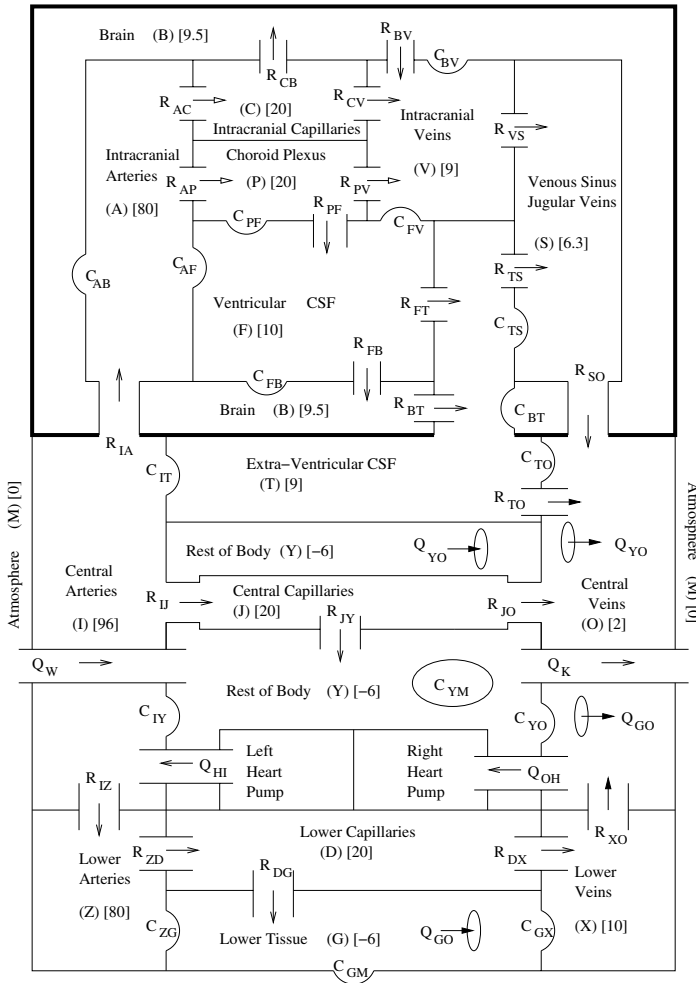


Fig. 1. The 16 compartment model. A filled arrow indicates a one-way flow and a hollow arrow indicates a pressure dependent resistance. Compartment labels are enclosed in parentheses with the spatially-averaged mean pressures in square brackets. The thick line indicates the cranial wall.

- All fluids are considered incompressible and isothermal.
- Pressure driven flows are laminar and related to pressure differences by

$$Q_{ij} = \frac{P_i - P_j}{R_{ij}} = Z_{ij}(P_i - P_j) = Z_{ij}P_{ij}, \quad (1)$$

where Q_{ij} is the flow from compartment i into compartment j , P_i and P_j are the spatially-averaged pressures of compartments i and j respectively, R_{ij} is the lumped resistance, Z_{ij} is the fluidity (inverse of R_{ij}), the pressure difference $P_{ij} = P_i - P_j$, and $R_{ij} = -R_{ji}$.

- In the case of fluid filtration from the capillaries into the interstitial space, the flow is governed by the Starling-Landis Equation

$$\text{Filtration} = K_{ct} ((P_c - P_t) - \sigma_{ct}(\pi_c - \pi_t)) = K_{ct}(P_{ct} - \sigma_{ct} \pi_{ct}), \quad (2)$$

where P_c is the capillary pressure, P_t is the interstitial fluid pressure, π_c is the blood plasma colloid osmotic pressure, π_t is the interstitial fluid colloid osmotic pressure, K_{ct} is the filtration coefficient, and σ_{ct} is the capillary membrane reflection coefficient. The notation for pressure difference has been extended to osmotic pressure differences by defining $\pi_{ct} = \pi_c - \pi_t$.

- The deformation of the membrane between adjacent compartments is a function of the change in pressure difference between these compartments;

$$\frac{dV_{ij}}{dt} = C_{ij} \frac{d(P_i - P_j)}{dt} = C_{ij} \frac{d(P_{ij})}{dt}, \quad (3)$$

where V_{ij} denotes the instantaneous volume of the 'cup' formed in the membrane at the interface of compartments i and j , C_{ij} denotes the compliance between these two compartments, and $C_{ij} = C_{ji}$

The system of governing equations is now obtained by invoking the conservation law

$$\text{flow rate in} - \text{flow rate out} = \text{rate of volume change} \quad (4)$$

in each compartment. In terms of pressure differences, this relation yields the following system of 13 differential equations and 3 scalar equations for the 16 body compartments:

- Central Artery Compartment (I):

$$Q_{HI} - (Z_{IJ}P_{IJ} + Z_{IZ}P_{IZ} + Z_{IA}P_{IA}) = C_{IT} \frac{dP_{IT}}{dt} - \frac{dV_{YI}}{dt}. \quad (5)$$

- Central Capillary Compartment (J):

$$Z_{IJ}P_{IJ} - (K_{JY}(P_{JY} - \sigma_{JY}\pi_{JY}) + Z_{JO}P_{JO}) = 0. \quad (6)$$

- Rest of Body Compartment (Y):

$$Q_W + K_{JY}(P_{JY} - \sigma_{JY}\pi_{JY}) - (Q_{YO} + Q_K) = C_{YM} \frac{dP_{YM}}{dt} + \frac{dV_{YI}}{dt} + \frac{dV_{YO}}{dt}. \quad (7)$$

- Central Venous Compartment (O):

$$\begin{aligned} & Z_{J0}P_{JO} + Z_{XO}P_{XO} + Z_{SO}P_{SO} + Z_{TO}P_{TO} + Q_{GO} + Q_{YO} - Q_{OH} \\ & = C_{TO} \frac{dP_{OT}}{dt} - \frac{dV_{YO}}{dt}. \end{aligned} \quad (8)$$

- Lower Artery Compartment (Z):

$$Z_{IZ}P_{IZ} - Z_{ZD}P_{ZD} = C_{ZG} \frac{dP_{ZG}}{dt}. \quad (9)$$

- Lower Capillary Compartment (D):

$$Z_{ZD}P_{ZD} - (Z_{DX}P_{DX} + K_{DG}(P_{DG} - \sigma_{DG}\pi_{DG})) = 0. \quad (10)$$

- Lower Tissue Compartment (G):

$$K_{DG}(P_{DG} - \sigma_{DG}\pi_{DG}) - Q_{GO} = C_{ZG} \frac{dP_{GZ}}{dt} + C_{GX} \frac{dP_{GX}}{dt} + C_{GM} \frac{dP_{GM}}{dt}. \quad (11)$$

- Lower Venous Compartment (X):

$$Z_{DX}P_{DX} - Z_{X0}P_{X0} = C_{GX} \frac{dP_{XG}}{dt}. \quad (12)$$

- Intracranial Artery Compartment (A):

$$Z_{IA}P_{IA} - (Z_{AC}P_{AC} + Z_{AP}P_{AP}) = C_{AB} \frac{dP_{AB}}{dt} + C_{AF} \frac{dP_{AF}}{dt}. \quad (13)$$

- Intracranial Capillary Compartment (C):

$$Z_{AC}P_{AC} - (Z_{CB}P_{CB} + Z_{CV}P_{CV}) = 0. \quad (14)$$

- Choroid Plexus Compartment (P):

$$Z_{AP}P_{AP} - (Z_{PF}P_{PF} + Z_{PV}P_{PV}) = C_{PF} \frac{dP_{PF}}{dt}. \quad (15)$$

- Intracranial Veins Compartment (V):

$$Z_{CV}P_{CV} + Z_{PV}P_{PV} + Z_{BV}P_{BV} - Z_{VS}P_{VS} = C_{BV} \frac{dP_{VB}}{dt} + C_{FV} \frac{dP_{VF}}{dt}. \quad (16)$$

- Venous Sinus - Jugular Veins Compartment (S):

$$Z_{VS}P_{VS} + Z_{TS}P_{TS} - Z_{SO}P_{SO} = C_{TS} \frac{dP_{ST}}{dt}. \quad (17)$$

- Ventricular CSF Compartment (F):

$$\begin{aligned} & Z_{PF}P_{PF} - (Z_{FB}P_{FB} + Z_{FT}P_{FT}) \\ &= C_{AF} \frac{dP_{FA}}{dt} + C_{PF} \frac{dP_{FP}}{dt} + C_{FB} \frac{dP_{FB}}{dt} + C_{FV} \frac{dP_{FV}}{dt}. \end{aligned} \quad (18)$$

- Extra-Ventricular CSF Compartment (T):

$$\begin{aligned} & Z_{FT}P_{FT} + Z_{BT}P_{BT} - (Z_{TS}P_{TS} + Z_{TO}P_{TO}) \\ &= C_{TS} \frac{dP_{TS}}{dt} + C_{BT} \frac{dP_{TB}}{dt} + C_{TO} \frac{dP_{TO}}{dt} + C_{IT} \frac{dP_{TI}}{dt}. \end{aligned} \quad (19)$$

- Brain Compartment (B):

$$\begin{aligned} & Z_{CB}P_{CB} + Z_{FB}P_{FB} - (Z_{BV}P_{BV} + Z_{BT}P_{BT}) \\ &= C_{AB} \frac{dP_{BA}}{dt} + C_{BV} \frac{dP_{BV}}{dt} + C_{FB} \frac{dP_{BF}}{dt} + C_{BT} \frac{dP_{BT}}{dt}. \end{aligned} \quad (20)$$

The terms dV_{YI}/dt and dV_{YO}/dt in the conservation equations for compartments Y, I, and O have been left intact in (5), (7), and (8). These volume changes include components that reflect the regulation of arterial pressure by the sympathetic nervous system. They are considered in section 2.3.3. The terms involving dP_M/dt in the conservation equations for compartments Y, and G (equations (7) and (11)) denote a volume change for which there is no compensation through an equal but opposite volume change in an adjacent body compartment. Specifically, these terms reflect volume increases (or decreases) into the ambient environment, which is considered infinitely large and unaffected by pressure changes within the body. This additional Ambient Environment compartment (M) is similar to the ground in an electrical circuit model. It will be maintained at a constant pressure value in exactly the same way that the ground voltage in a circuit model is given a prescribed value relative to which all other values are gauged. Accordingly, the ambient environmental pressure P_M is fixed here at a constant reference value of zero mmHg. If this is not appropriate for a situation being studied, or if the ambient pressure changes with time, then P_M must be considered as a forcing term in the system of equations.

The set of governing equations may be summed to derive the following constraint regarding compliances between the body and the external environment:

$$(Q_W - Q_K) + (Q_{HI} - Q_{OH}) = C_{YM} \frac{dP_{YM}}{dt} + C_{GM} \frac{dP_{GM}}{dt}. \quad (21)$$

If cardiac output equals cardiac uptake ($Q_{HI} = Q_{OH}$) and the atmospheric pressure is constant, equation (21) simplifies to

$$Q_W - Q_K = C_{YM} \frac{dP_Y}{dt} + C_{GM} \frac{dP_G}{dt}. \quad (22)$$

If, in addition, $Q_W = Q_K = 0$ or fluid intake equals fluid discharge ($Q_W = Q_K$), then (22) implies as expected that the net volume change of the entire body system must be zero. Furthermore, if $Q_W > Q_K$, as will initially be the case when a glass of water is consumed, the net volume of the body will increase. By (22), one of the internal compartmental pressures: P_G , or most likely P_Y , must now increase. However, if as will be the case, C_{YM} is large, the resultant pressure increase in compartment Y due to the volume input from the ambient environment will be small.

2.2. Parameter expressions and calibrations

The fluidities in equation (1) that relate flows to pressure differences are derived in section 2.2.1. The filtration and reflection coefficients of equation (2) are calibrated in section 2.2.2. The compliances in equation (3) that relate pressure differences and volume adjustments are calibrated in section 2.2.3.

2.2.1. Fluidities

Each constant fluidity Z_{ij} between arbitrary adjacent compartments i and j may be calculated by substituting the mean pressures and the mean flow rates into equation (1) and solving for Z_{ij} , giving

$$Z_{ij} = \frac{\bar{Q}_{ij}}{\bar{P}_i - \bar{P}_j}. \quad (23)$$

Therefore, once the mean flows and pressures are estimated from physical data, the associated constant fluidities may be calculated from (23). Some model fluidities are pressure dependent, and a discussion of appropriate expressions for these fluidities will be postponed until sections 2.3.2, 2.3.3, and 2.3.4 where CSF, cerebrovascular, sympathetic nervous system, and cardiac autoregulation mechanisms are modeled. However, even for a non-constant fluidity, a mean scale value may still be calculated from (23). In the calibrations that follow, mean flows and pressures reflect physiological values for an average human in a lying down (supine) position. Mean pressures (in mmHg) for this state are displayed in square brackets in Figure 1.

To estimate mean flows, it will be assumed that compartmental volumes remain constant in the mean state. Compartmental pressures are certainly pulsatile, so the system will have a mean state, but not a steady state. However, since volume changes are related to pressure differences between adjacent compartments, if pressures in adjacent compartments move in tandem in the mean state, volumes will remain unchanged. Therefore, for a given compartment, if all but one of the mean flows are known, the final mean flow may be determined from maintaining constant volume. Further, once mean flows into and out of a given compartment are determined, these values provide data for flows in the adjacent compartments. While many flows can be estimated from data available in published literature, most mean flow calibrations must make use of the constant volume assumption.

As a starting point for the calibration of mean flows, consider the percentages of cardiac output Q_{HI} that exit the central arteries into the three peripheral vascular systems: A, J or Z. These percentages, in decimal form, are given below with data references noted in square brackets.

$$p_{ia} = .15, \quad = \% \text{ of cardiac output into intracranial region [11]} \quad (24)$$

$$p_{iz} = .25, .35, \quad = \% \text{ of cardiac output into lower region [7,24]} \quad (25)$$

$$p_{ij} = 1 - (p_{ia} + p_{iz}), \quad = \% \text{ of cardiac output into rest of body} \quad (26)$$

Additional helpful percentages and ratios include

$$p_{pf} = .70, \quad = \% \text{ of CSF formation from the choroid plexus [32]} \quad (27)$$

$$\lambda = 250, \quad = \bar{Q}_{AC} / \bar{Q}_{AP} \text{ [16]} \quad (28)$$

$$p_{ts} = .80, \quad = \% \text{ of CSF drained into venous sinus [41]} \quad (29)$$

Literature values give the following mean flows in ml/min:

$$\bar{Q}_{HI} = 5000, 6600, 6900, \quad \text{Cardiac output [11,24,26]} \quad (30)$$

$$\bar{Q}_{CF} = 2, \quad \text{Total capillary filtration (with 2/3 from liver and intestines) [11]} \quad (31)$$

$$\bar{Q}_{JY} = \bar{Q}_{CF} \left(\frac{2}{3} + \frac{1}{3} \frac{p_{ij}}{p_{ij} + p_{iz}} \right),$$

Total capillary filtration into central tissue [11] (32)

$$\bar{Q}_{DG} = \frac{1}{3} \frac{p_{iz}}{p_{ij} + p_{iz}} \bar{Q}_{CF}, \quad \text{Total capillary filtration into lower tissue [11]} \quad (33)$$

$$\bar{Q}_F = .35, \quad \text{Total CSF formation [11,32]} \quad (34)$$

$$\bar{Q}_{BV} = .001, \quad \text{Imbalance of diffusion on venule side of cerebrovasculature [36]} \quad (35)$$

$$\bar{Q}_{FB} = .044, \quad \text{Flow of CSF through the Virchow-Robins Space [36]} \quad (36)$$

All of the remaining mean flows in the model may now be calibrated based on equations (24) through (36) by invoking the constant volume assumption in each compartment during the mean state. The calibration procedure yields the mean flows:

Central Body Mean Flows

$$\bar{Q}_{OH} = \bar{Q}_{HI} \quad \text{from cardiac output} = \text{cardiac input [11]} \quad (37)$$

$$\bar{Q}_{IA} = p_{ia} \bar{Q}_{HI} \quad \text{from equation (24)} \quad (38)$$

$$\bar{Q}_{IZ} = p_{iz} \bar{Q}_{HI} \quad \text{from equation (25)} \quad (39)$$

$$\bar{Q}_{IJ} = \bar{Q}_{HI} - (\bar{Q}_{IA} + \bar{Q}_{IZ}) \quad \text{from constant volume in I} \quad (40)$$

$$\bar{Q}_{JO} = \bar{Q}_{IJ} - \bar{Q}_{JY} \quad \text{from constant volume in J} \quad (41)$$

$$\bar{Q}_{YO} = \bar{Q}_{JY} \quad \text{from constant volume in Y} \quad (42)$$

Lower Body Mean Flows

$$\bar{Q}_{ZD} = \bar{Q}_{IZ} \quad \text{from constant volume in Z} \quad (43)$$

$$\bar{Q}_{GO} = \bar{Q}_{DG} \quad \text{from constant volume in G} \quad (44)$$

$$\bar{Q}_{DX} = \bar{Q}_{ZD} - \bar{Q}_{DG} \quad \text{from constant volume in D} \quad (45)$$

$$\bar{Q}_{XO} = \bar{Q}_{DX} \quad \text{from constant volume in X} \quad (46)$$

Intracranial Mean Flows

$$\bar{Q}_{AP} = \bar{Q}_{IA}/(\lambda + 1) \quad \text{from constant volume in A and equation (28)} \quad (47)$$

$$\bar{Q}_{AC} = \lambda \bar{Q}_{AP} \quad \text{from equation (28)} \quad (48)$$

$$\bar{Q}_{PF} = p_{pf} \bar{Q}_F \quad \text{from equation (27)} \quad (49)$$

$$\bar{Q}_{CB} = (1 - p_{pf}) \bar{Q}_F + \bar{Q}_{BV} \quad \text{from } \bar{Q}_{CB} - \bar{Q}_{BV} = (1 - p_{pf}) \bar{Q}_F \quad (50)$$

$$\bar{Q}_{CV} = \bar{Q}_{AC} - \bar{Q}_{CB} \quad \text{from constant volume in C} \quad (51)$$

$$\bar{Q}_{PV} = \bar{Q}_{AP} - \bar{Q}_{PF} \quad \text{from constant volume in P} \quad (52)$$

$$\bar{Q}_{VS} = \bar{Q}_{CV} + \bar{Q}_{PV} + \bar{Q}_{BV} \quad \text{from constant volume in V} \quad (53)$$

$$\bar{Q}_{BT} = \bar{Q}_{CB} + \bar{Q}_{FB} - \bar{Q}_{BV} \quad \text{from constant volume in B} \quad (54)$$

$$\overline{Q}_{FT} = \overline{Q}_{PF} - \overline{Q}_{FB} \quad \text{from constant volume in F} \quad (55)$$

$$\overline{Q}_{TS} = p_{ts} \overline{Q}_F \quad \text{from equation (29)} \quad (56)$$

$$\overline{Q}_{TO} = (1 - p_{ts}) \overline{Q}_F \quad \text{from constant volume in T} \quad (57)$$

$$\overline{Q}_{SO} = \overline{Q}_{VS} + \overline{Q}_{TS} \quad \text{from constant volume in S} \quad (58)$$

Equation (49) states that 70 % of the CSF formation comes from the choroid plexus [32] and equation (50) states that the remaining CSF formation comes as a filtrate from the capillaries through the brain via the Virchow-Robins system [32] minus the amount reabsorbed at the venule side of the capillaries (Q_{BV}). Notice that, as should be the case, $\overline{Q}_{BT} + \overline{Q}_{FT} = \overline{Q}_F$.

2.2.2. Reflection and filtration coefficients

There are two locations in the model where fluid flow is governed by the Starling-Landis equation (2). These flows in the central and lower body are

$$Q_{JY} = K_{JY} ((P_J - P_Y) - \sigma_{JY}(\pi_J - \pi_Y)) \quad (59)$$

$$Q_{DG} = K_{DG} ((P_D - P_G) - \sigma_{DG}(\pi_D - \pi_G)), \quad (60)$$

denoting the flow from the capillaries into the tissue subunits of the central and lower body regions, respectively. Solving these relations for the filtration coefficients in the mean state implies

$$K_{JY} = \frac{\overline{Q}_{JY}}{((\overline{P}_J - \overline{P}_Y) - \sigma_{JY}(\overline{\pi}_J - \overline{\pi}_Y))} \quad (61)$$

$$K_{DG} = \frac{\overline{Q}_{DG}}{((\overline{P}_D - \overline{P}_G) - \sigma_{DG}(\overline{\pi}_D - \overline{\pi}_G))}. \quad (62)$$

The mean flows on the right hand side of these equations have been calculated in the previous section, and the mean values adopted for the compartmental pressures P_J , P_Y , P_D , and P_G are indicated in square brackets in Figure 1. Thus, to determine the filtration coefficients K_{JY} and K_{DG} , it is only necessary to calibrate scale values for the mean colloid osmotic pressures and the reflection coefficients.

Mean interstitial fluid colloid osmotic pressure is given by

$$\overline{\pi}_Y = \overline{\pi}_G = 8 \text{ mmHg} \quad [11,31]. \quad (63)$$

and blood plasma colloid osmotic pressure by

$$\overline{\pi}_J = \overline{\pi}_D = 28 \text{ mmHg} \quad [11,31]. \quad (64)$$

Notice that these values are invariant with respect to central or lower regions. This is not the case, however, with the reflection coefficients σ_{JY} and σ_{DG} . The reflection coefficient in the legs is estimated to be approximately 0.9 [34,40] while the coefficient of the upper body is less than this value [31]. This is reflected by the assignments

$$\sigma_{JY} = .8 \quad (65)$$

$$\sigma_{DG} = .9 \quad (66)$$

The filtration coefficients K_{JY} and K_{DG} in equations (61) and (62) are now readily determined.

2.2.3. Compliances

In this section, the various compliances in equation (3) that relate volume adjustments to pressure differences will be calculated. In the intracranial region, compartmental volume increases are restricted by the rigid cranial wall. Consequently, compartmental compliances must be pressure dependent and diminish to zero as pressure differences become large. On the other hand, in extracranial regions, to lowest order compliances may consistently be considered constant, approximating a linear relationship between pressure differences and volume adjustments. The present intracranial pressure-dependent compliances are extensions of those derived in [38], while the constant extra-cranial compliances will be derived from estimations of the volume and distensibility of each compartment.

Intracranial, Pressure-Dependent Compliances: In the simplified 4-compartment whole-body model for CSF dynamics described in [38], there are only two pressure difference-dependent compliances. They allow volume adjustments between the CSF and arterial blood and between the CSF and venous blood. These compliances have the general form described by the relation

$$C_{ij}^4(P_{ij}) = C_{ij}^o e^{-r_{ij}|P_{ij}|^{\alpha_{ij}}}, \quad (67)$$

where $P_{ij} = P_i - P_j$, and the subscripts i and j take the values C_{af}^4 (for arterial/CSF compliance) and C_{fv}^4 (for CSF/venous compliance). For both pairs of index values, coefficients and parameters in equation (67) are given by

$$C_{fv}^o = 6.5333, \quad r_{fv} = 0.633431 \quad \alpha_{fv} = 0.604229 \quad (68)$$

$$C_{af}^o = 1.82745, \quad r_{af} = 0.817102 \quad \alpha_{af} = 0.869393 \quad (69)$$

This 4-compartment model contains an additional constant compliance between the CSF and the rest of the body (g), which is approximated as

$$C_{fg}^4 = 0.13333. \quad (70)$$

This feature represents the interface of extra-cranial CSF in the spinal theca with the rest of the body. It also acts as a background compliance so that the total CSF compliance can never reach machine zero in simulations.

In the present 16 compartment model, the division of the body's cerebrospinalfluid space is considerably more refined. Hence, the three CSF compliances in the simple four compartment model of [38] must be appropriately apportioned among the compliances of the present model. Three decimal percentages may be introduced to describe this allocation of C_{fv}^4 :

$$p_{fv} = .164 \quad \text{percentage of } C_{fv}^4 \text{ allocated to } C_{FV} \quad (71)$$

$$p_{to} = .214 \quad \text{percentage of } C_{fv}^4 \text{ allocated to } C_{TO} \quad (72)$$

$$p_{ts} = .622 \quad \text{percentage of } C_{fv}^4 \text{ allocated to } C_{TS} \quad (73)$$

Equations (71–73) reflect the fact that total CSF volume is approximately 140 ml, 23 of which is found in the ventricles, 30 in the spinal cord subarachnoid space (theca)

and the remainder in the cerebral cisterns and subarachnoid space [32]. Thus, if the distensibility of the membrane is similar in these three different components of CSF, then C_{fv} is $23/140 = .164$ of C_{fv}^4 as indicated by p_{fv} in equation (71). This same technique yields the values in equations (72) and (73). The compliance C_{PF} is excluded in this division of C_{fv}^4 as the choroid plexus capillaries are known to dilate and constrict in order to maintain a constant pressure difference between these capillaries and ventricular CSF [11]. This maintains a constant generation rate of CSF from the choroid plexus at normal pressure values [39]. Consequently, a value for the compliance C_{PF} is irrelevant in the absence of a pressure-difference change.

The ratios that lead to equations (71)–(73) also imply the following percentages describing the allocation of C_{af}^4 from [38]:

$$p_{af} = .786 \quad \text{percentage of } C_{af}^4 \text{ allocated to } C_{AF} \quad (74)$$

$$p_{it} = .214 \quad \text{percentage of } C_{af}^4 \text{ allocated to } C_{IT} \quad (75)$$

The background compliance C_{fg}^4 from [38] is now divided between venous and arterial interfaces based on systemic venous volume being four times that of arterial volume [11], giving

$$C_{venous} = .8 C_{fg}^4 \quad (76)$$

$$C_{arterial} = .2 C_{fg}^4 \quad (77)$$

The CSF-related compliances may now be calculated based on the above percentages as:

$$C_{FV}(P_{FV}) = .95 p_{fv} (C_{fv}^4(P_{FV}) + C_{venous}) \quad \bar{C}_{FV} = 0.557868 \text{ ml/mmHg}$$

$$C_{FB}(P_{FB}) = .05 p_{fv} (C_{fv}^4(P_{FB}) + C_{venous}) \quad \bar{C}_{FB} = 0.036255 \text{ ml/mmHg}$$

$$C_{TS}(P_{TS}) = 0.95 p_{ts} (C_{fv}^4(P_{TS}) + C_{venous}) \quad \bar{C}_{TS} = 1.27626 \text{ ml/mmHg}$$

$$C_{BT}(P_{BT}) = 0.05 p_{ts} (C_{fv}^4(P_{BT}) + C_{venous}) \quad \bar{C}_{BT} = 0.137057 \text{ ml/mmHg}$$

$$C_{TO}(P_{TO}) = p_{to} (C_{fv}^4(P_{TO}) + C_{venous}) \quad \bar{C}_{TO} = 0.200936 \text{ ml/mmHg}$$

$$C_{AF}(P_{AF}) = p_{af} (C_{af}^4(P_{AF}) + C_{arterial}) \quad \bar{C}_{AF} = 0.0261999 \text{ ml/mmHg}$$

$$C_{IT}(P_{IT}) = p_{it} (C_{af}^4(P_{IT}) + C_{arterial}) \quad \bar{C}_{IT} = 0.00571427 \text{ ml/mmHg}$$

where again, the pressure difference $P_i - P_j$ is denoted P_{ij} and the scale value $\bar{C}_{ij} = C_{ij}(\bar{P}_i - \bar{P}_j) = C_{ij}(\bar{P}_{ij})$. The compliance C_{BT} , introduced to incorporate volume adjustments between the brain and subarachnoid CSF, is allocated 5% of C_{TS} . This states that of the bulk intracranial compliance in compartment T, 95% is allocated to the interface with the highly distensible venous sinus veins and only 5% to the interface with the less distensible brain tissue. A similar allocation is made for the bulk intracranial compliance of the ventricular CSF compartment F with respect to the intracranial veins and the brain tissue.

Finally, brain/vascular compliances $C_{AB}(P_{AB})$ and $C_{BV}(P_{BV})$ are defined by reference to similar CSF/vascular compliances as:

$$C_{AB}(P_{AB}) = C_{AF}(P_{AB}) \quad \bar{C}_{AB} = 0.0209523 \text{ ml/mmHg}$$

$$C_{BV}(P_{BV}) = C_{FV}(P_{BV}) \quad \bar{C}_{BV} = 0.688845 \text{ ml/mmHg.}$$

Extra-cranial Compliances: When calculating extra-cranial compliances it is advantageous to first determine the total compliance of each compartment. This quantity will be denoted by C_i with the subscript indicating the compartment. This type of compliance can be described by the relation

$$\text{Total Compartmental Compliance} = \frac{\text{Increase in Compartmental Volume}}{\text{Increase in Compartmental Pressure}} \quad (78)$$

and may be experimentally determined by measuring the pressure change that is induced by an estimated volume change and then taking the inverse of this ratio. Unfortunately, clinical data does not exist for determination of all of the compliances required for the current model. However, there is information in the literature regarding volumes and distensibilities. These are related to compliance by

$$\text{Compliance} = \text{Distensibility} \cdot \text{Volume}. \quad (79)$$

Therefore, total compartmental compliance may be calculated from total compartmental volume (denoted V_i) and compartmental distensibility (denoted D_i) through equation (79). However, before calculating compartmental volumes and distensibilities it is useful to describe how the resulting total compartmental compliances will be allocated to the local inter-compartmental compliances.

Estimations of the local compliances are made by requiring that the sum of the relevant local compliances must equal the total compliance being apportioned. With this restriction, the model's predicted compartmental pressure changes induced by known volume changes should agree with experimental data. Based on this principle, the apportionment of total compliances among local compliances is described by

Central, Local Compliances:

$$C_{IY} = \text{Max}[C_I - \bar{C}_{IT}, 0] \text{ ml/mmHg} \quad (80)$$

$$C_{YO} = \text{Max}[C_O - \bar{C}_{TO}, 0] \text{ ml/mmHg} \quad (81)$$

$$C_{YM} = \text{Max}[C_Y - (C_{IY} + C_{YO}), 0] \text{ ml/mmHg} \quad (82)$$

Lower, Local Compliances:

$$C_{ZG} = C_Z \text{ ml/mmHg} \quad (83)$$

$$C_{GX} = C_X \text{ ml/mmHg} \quad (84)$$

$$C_{GM} = \text{Max}[C_G - (C_{ZG} + C_{GX}), 0] \text{ ml/mmHg} \quad (85)$$

Here, the $\text{Max}[\ , \]$ function is used to ensure that no negative compliances occur in the model. For the particular choices of total compliances here, this function is not needed, but it is included above as it may be required if total tissue compliances are calculated to be much smaller.

Volumes: Total blood volume (V_{blood}) is estimated at 5000 ml [11] and 5600 ml [24], where blood plasma makes up about 60% of this [11]. The relative volumes of systemic veins, arteries and capillaries are [11]

$$V_{sa} = .16 V_{blood} \quad \text{systemic artery volume} \quad (86)$$

$$V_{sv} = .64 V_{blood} \quad \text{systemic vein volume} \quad (87)$$

$$V_{sc} = .04 V_{blood} \quad \text{systemic capillary volume} \quad (88)$$

$$V_{pulm} = .09 V_{blood} \quad \text{pulmonary system volume} \quad (89)$$

$$V_{heart} = .07 V_{blood} \quad \text{heart-blood volume} \quad (90)$$

These values are based on estimates that the systemic arteries comprise 13% of the blood volume while the systemic arterioles and capillaries comprise 7%. In the present model, arteriole volume is lumped with the arteries, and hence 3% of the arteriole/capillary space in [11] is shifted here into the artery compartment resulting in the percentages above. It should also be noted that these percentages imply that systemic venous volume is four times that of systemic artery volume.

As a next step, arterial and venous volumes must be allocated between the intracranial, lower, and central compartments. Estimates for this distribution are given below. It should be emphasized that these are percentages of the systemic blood and exclude the blood volumes in the heart and pulmonary system.

$$pV_{cran} = .07 \quad \text{percentage of systemic blood, intracranial region [7]} \quad (91)$$

$$pV_{lower} = .40 \quad \text{percentage of systemic blood, lower region [28]} \quad (92)$$

$$pV_{central} = .53 \quad \text{percentage of systemic blood, central region [28]} \quad (93)$$

The above percentages lead to the following volumes for the extra-cranial, vascular compartments:

$$V_Z = pV_{lower} V_{sa} \quad = \text{lower artery volume} \quad (94)$$

$$V_I = pV_{central} V_{sa} \quad = \text{central artery volume} \quad (95)$$

$$V_X = pV_{lower} V_{sv} \quad = \text{lower vein volume} \quad (96)$$

$$V_O = pV_{central} V_{sv} \quad = \text{central vein volume} \quad (97)$$

$$V_D = pV_{lower} V_{sc} \quad = \text{lower capillary volume} \quad (98)$$

$$V_J = pV_{central} V_{sc} \quad = \text{central capillary volume.} \quad (99)$$

The volumes of the tissue and rest of body compartments are now calculated based on interstitial fluid volume and intracellular fluid volume. Total interstitial fluid volume is estimated in [11] to be 12 L, while total intracellular fluid volume is estimated to be 28 L. Considering that approximately 2 L of the intracellular fluid is contained in the blood cells, the following volume assignments can be made:

$$V_{inter} = 12000 \text{ ml} \quad = \text{interstitial fluid volume} \quad (100)$$

$$V_{intra} = 26000 \text{ ml} \quad = \text{intracellular fluid volume} \quad (101)$$

With these volume assignments and the percentages in equations (92)–(93), estimates for lower tissue and rest-of-body volumes become:

$$V_G = pV_{lower}(V_{inter} + V_{intra}) = \text{lower tissue volume} \quad (102)$$

$$V_Y = pV_{central}(V_{inter} + V_{intra}) + V_{pulm} = \text{rest of body volume} \quad (103)$$

Distensibilities: Estimations for the pressure-strain modulus are given by Milnor [24] and Nichols and O'Rourke [27] for various branches of the systemic arteries. From this data, the distensibility of the various vessels can be calculated. Of interest here are the calculated distensibilities for the ascending aorta and the femoral artery, represented in the model by D_I and D_Z . Milnor's data [24] suggests that D_I is $0.0036225 \text{ mmHg}^{-1}$ and D_Z is $0.00101 \text{ mmHg}^{-1}$ while Nichols and O'Rourke data [27] suggests D_I is $0.00320141 \text{ mmHg}^{-1}$ and D_Z is $0.00237912 \text{ mmHg}^{-1}$. Averaging these values results in the assignments

$$D_I = 0.00341196 \quad (104)$$

$$D_Z = 0.00169456 . \quad (105)$$

Since the central veins are 8 times as distensible as central arteries [11], D_O is calculated accordingly by

$$D_O = 8 D_I. \quad (106)$$

There are some suggestions [42] that the upper venous distensibility may be larger than that of the lower leg, but these results are inconclusive. Therefore, lower venous distensibility is set to

$$D_X = D_O. \quad (107)$$

Consistent with [35], the capillary compartments C, J, and D are considered non-deformable.

The distensibility of the lower tissue compartment is assigned a weighted average of the interfacing vein and artery distensibilities. Since the veins have 4 times the volume of the arteries, these weights are used in

$$D_G = \frac{D_Z + 4 D_X}{5} = 0.0221754 \text{ (ml/mmHg)/ml} \quad (108)$$

Finally, the distensibility of the rest-of-body compartment (Y) is also a weighted average based on its composition:

$$\begin{aligned} D_Y &= \frac{pV_{central}(V_{inter} + V_{intra})D_G + (\frac{4}{5} V_{pulm})D_O + (\frac{1}{5} V_{pulm})D_I}{V_Y} \\ &= 0.0221838 \text{ (ml/mmHg)/ml} \end{aligned} \quad (109)$$

The distensibilities of the extra-cranial compartments have now been determined. Combined with the volumes of the previous section, each extra-cranial compartment now has an associated total compliance equal to the product of its associated volume and distensibility.

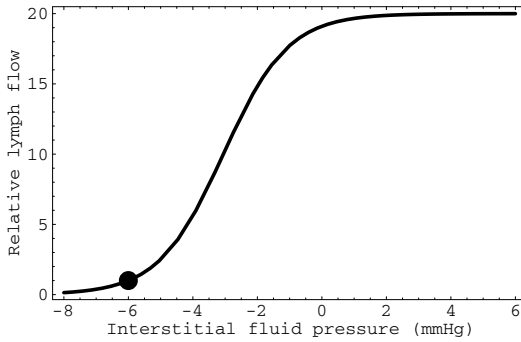


Fig. 2. The relationship between interstitial fluid pressure and relative lymph flow.

2.3. Forcing and regulatory mechanisms

2.3.1. Lymphatic autoregulation

The lymphatic system is represented in the present model through the flows Q_{YO} and Q_{GO} . These flows provide pathways through which interstitial fluid can move directly from the interstitium to the central venous system. Unlike the flows between adjacent compartments, which are driven by pressure differences, the lymphatic flow is governed almost exclusively by the interstitial fluid pressure [11]. This flow increases 20 fold at interstitial fluid pressures near 4 mmHg from the corresponding flow at an interstitial pressure of -6 mmHg. Below this interstitial fluid pressure value, lymphatic flow ceases [11]. The relative lymphatic curve is modeled by the logistic expression

$$P_{lymph}(x) = \frac{M}{1 + (M - 1)e^{-r(x+6)}}, \quad \text{where } M = 20 \text{ and } r = 1 \quad (110)$$

This function, depicted in Figure 2, defines the relative lymph flow in terms of interstitial pressure. The large dot in Figure 2 denotes the mean pressure of interstitial fluid in the model. Conversion of this relationship to the actual lymphatic flows Q_{GO} and Q_{YO} is accomplished by defining

$$Q_{GO}(t) = \frac{P_{lymph}(P_G)\bar{Q}_{GO}}{P_{lymph}(\bar{P}_G)}, \quad (111)$$

$$Q_{YO}(t) = \frac{P_{lymph}(P_Y)\bar{Q}_{YO}}{P_{lymph}(\bar{P}_Y)}. \quad (112)$$

In this manner, the mean flow is maintained at the mean pressure and can increase or decrease accordingly. Based on equation (110), Q_{GO} can increase from a mean flow of about 0.24 ml/min to 4.7 ml/min while Q_{YO} can increase from 1.76 ml/min to 35 ml/min.

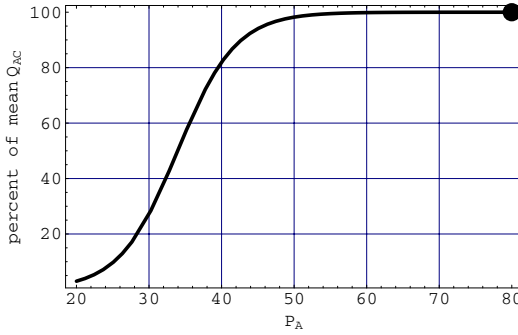


Fig. 3. The percent reduction in Q_{AC} with respect to P_A .

2.3.2. *Intracranial autoregulation*

Blood supply and CSF production is well regulated in the human intracranial system [11,32]. This auto-regulation is achieved by the dilation and constriction of the blood vessels induced by factors such as carbon dioxide concentration, hydrogen ion concentration, oxygen concentration and intracranial pressures. The model incorporates such auto-regulation in the form of pressure sensitive fluidities depicting either vessel constriction in the form of a reduced fluidity or dilation in form of increased fluidity.

Blood flow into the cerebral capillaries is auto-regulated by a pressure dependent fluidity Z_{AC} defined by

$$Z_{AC} = \frac{F(P_A)}{P_A - P_C}, \tag{113}$$

where $F(P_A)$ is a logistic expression defined by

$$F(P_A) = \bar{Q}_{AC} \frac{M}{1 + (M - 1)e^{r(\bar{P}_A - P_A)}} \quad \text{with } M = 1.00001 \text{ and } r = 0.25. \tag{114}$$

This implies that $Q_{AC} = Z_{AC}(P_A - P_C) = F(P_A)$ and cerebral blood flow is thus determined almost entirely by intracranial artery pressure and does not diminish significantly until this pressure drops below 50 mmHg. The relationship between Q_{AC} and P_A is displayed in Figure 3.

Blood flow into the choroid plexus is regulated by a pressure-difference dependent fluidity Z_{AP} defined by

$$Z_{AP} = \frac{\bar{Q}_{AP}}{(P_A - P_P)} \cdot G(P_{perf}) \tag{115}$$

where the multiplier $G(P_{perf})$ in (115) is a function of the perfusion pressure $P_{perf} = P_A - P_B$ that is unity when P_{perf} exceeds 55 mmHg and then falls linearly to zero below this value. This implies that

$$Q_{AP} = Z_{AP} \cdot (P_A - P_P) = \bar{Q}_{AP} \cdot G(P_{perf}). \tag{116}$$

The multiplier G has been included in (115) to model the fact that CSF production in the choroid plexus scales with blood flow, remains nearly constant over a wide range of pressures, and is decreased as a function of the magnitude of the perfusion pressure when P_{perf} falls below 50 to 60 mmHg [39]. From (116), blood flow into the choroid plexus remains constant unless perfusion pressure falls to a low level.

Over the wide range of normal pressures, the production of CSF is auto-regulated at the venous side of the choroid plexus capillaries by the pressure dependent fluidity Z_{PV} defined by

$$Z_{PV} = \frac{\bar{Q}_{AP} \cdot G(P_{perf}) - Z_{PF} \cdot (P_P - P_F)}{P_P - P_V}. \quad (117)$$

When $P_{perf} \geq 55$, this expression for Z_{PV} will maintain a constant pressure difference between the choroid plexus and the ventricular CSF. Substituting Z_{PV} with $G = 1$ into the governing equation for the choroid plexus, equation (15) reduces to

$$C_{PF} \frac{dP_{PF}}{dt} = 0. \quad (118)$$

Since the compliance C_{PF} must be non-zero to account for the known ability of the Choroid Plexus to transmit pressure pulsations to the ventricular CSF [35], the governing equation for the choroid plexus compartment becomes simply

$$\frac{dP_{PF}}{dt} = 0. \quad (119)$$

This implies a constant pressure difference between the choroid plexus and ventricular CSF is maintained by (117) for $P_{perf} \geq 55$ mmHg. Therefore

$$Q_{PF} = Z_{PF} \cdot (P_P - P_F) = Z_{PF} (\bar{P}_P - \bar{P}_F) = \bar{Q}_{PF}. \quad (120)$$

Since for pressures in the normal range, CSF production in the choroid plexus is proportional to P_{PF} [39], constant CSF production from the choroid plexus is thus achieved. Equation (119) also eliminates the need to estimate C_{PF} in this model as occurrences of this parameter are always multiplied by either dP_{PF}/dt or dP_{FP}/dt .

Using the above results, it can now be demonstrated how Z_{PV} autoregulates CSF production for $P_{perf} \geq 55$ mmHg. Substituting \bar{Q}_{PF} for $Z_{PF} \cdot (P_P - P_F)$ in equation (117) and noting that $\bar{Q}_{AP} - \bar{Q}_{PF} = \bar{Q}_{PV}$ results in the equalities:

$$Z_{PV} = \frac{\bar{Q}_{PV}}{P_P - P_V} = \frac{\bar{Q}_{PV}}{(P_P - P_F) + (P_F - P_V)} = \frac{\bar{Q}_{PV}}{\bar{Q}_{PF} / Z_{PF} + (P_F - P_V)}. \quad (121)$$

The last term in this expression reveals the relationship between Z_{PV} and P_F . Physiologically, Z_{PV} should decrease with increasing CSF pressure (P_F) causing an increase in choroid plexus pressure and maintaining constant CSF production across Z_{PF} . It is quite clear from the last equality in (121) that this is indeed the case.

These autoregulatory mechanisms may be substituted into (13) to (16) and (18) to obtain the governing equations for compartments A, C, P, V, and F.

2.3.3. Regulation by the sympathetic nervous system (SNS)

The sympathetic nervous system (SNS) is associated with reflex mechanisms that act to maintain levels of arterial pressure and cardiac output if arterial pressure falls. This section deals with the portions of the model that represent the capacity of the SNS to rapidly increase arterial pressure by constricting both the arterioles and the large vascular vessels. The model's regulation of cardiac output by the SNS will be developed in section 2.3.4.

The Large Vessel Constrictive Response (SNSc):

As noted in [11], if arterial pressure falls, the large vessels of the circulation in the central body, especially the veins, strongly constrict to cause a rapid increase in arterial pressure. This mechanism is included in the current model by placing active interfaces between the central compartment Y and the central vascular compartments I and O. Forcing terms in the conservation equation for compartment Y now force the volume cups at the interfaces to push into the I and O compartments when arterial pressure diminishes, modeling the SNS large vessel constriction mechanism.

The conservation equation in compartment Y is described by

$$\frac{dV_Y}{dt} = \frac{dV_{YO}}{dt} + \frac{dV_{YI}}{dt} + \frac{dV_{YM}}{dt} = Q_{JY} - Q_{YO} \quad (122)$$

where the second equality determines the equation. Here, the volume change dV_{YM}/dt between compartment Y and the external environment M, as in (3), is simply proportional to the change in pressure difference dP_{YM}/dt . However, dV_{YO}/dt and dV_{YI}/dt involve both changes in the pressure differences dP_{YO}/dt and dP_{YI}/dt , respectively, and a forcing term describing the active compliance between Y and O and between Y and I, respectively. In particular,

$$\frac{dV_{YO}}{dt} = C_{YO} \frac{dP_{YO}}{dt} + F_{YO}(t) \quad \text{with} \quad F_{YO}(t) = -24P'_I \quad (123)$$

and

$$\frac{dV_{YI}}{dt} = C_{YI} \frac{dP_{YI}}{dt} + F_{YI}(t) \quad \text{with} \quad F_{YI}(t) = -8P'_I \quad (124)$$

The governing differential equation in compartment Y is now obtained by replacing dV_{YO}/dt and dV_{YI}/dt in equation (7) by the expressions (123) and (124). Similarly, for the governing equations in compartments O and I, dV_{YO}/dt is replaced in (8) by (123) and dV_{YI}/dt is replaced in (5) by (124), respectively.

The Arteriole Constrictive Response (SNSz):

A second SNS pressure regulation mechanism involves constriction of the arterioles in most parts of the body (excluding the brain and heart) when central artery pressure drops. This causes an increase in arterial pressure through an increase in the total peripheral resistance. When the arterial pressure drop is severe enough to compromise blood flow to the brain, this regulatory response is extreme, and has been termed a "last-ditch stand" in [11].

To model this portion of the SNS regulatory response, two multipliers are defined for the artery-capillary fluidities Z_{IJ} and Z_{ZD} . These variable resistances are of the form

$$Z_{IJ} = \frac{\bar{Q}_{IJ}}{\bar{P}_I - \bar{P}_J} \cdot SNSz_1(P_I) \cdot SNSz(Q_{AC}). \quad (125)$$

and

$$Z_{ZD} = \frac{\bar{Q}_{ZD}}{\bar{P}_Z - \bar{P}_D} \cdot SNSz_1(P_I) \cdot SNSz(Q_{AC}). \quad (126)$$

The first multiplier,

$$SNSz_1(P_I) = \frac{P_I}{\bar{P}_I}, \quad (127)$$

is a function of central body artery pressure that increases resistance if P_I falls below its mean level. The second multiplier, which is a function of the cerebral blood flow Q_{AC} , is defined by

$$SNSz(Q_{AC}) = \frac{M}{1 + (M - 1)e^{r(\bar{Q}_{AC} - Q_{AC})}} \quad \text{where } M = 1.1 \text{ and } r = 0.02. \quad (128)$$

This multiplier models the last-ditch stand when cerebral blood flow is significantly reduced. $SNSz$ remains close to unity (not activated) until arterial pressure drops to a level where Q_{AC} is affected. At this point, $SNSz$ drops sharply, dramatically increasing the resistances R_{IJ} and R_{ZD} .

2.3.4. Cardiac forcing and regulation

The major source of forcing in the present whole-body model comes from the heart and involves the cardiac output Q_{HI} and cardiac uptake Q_{OH} . As noted in [11], “.. all the extra blood that flows into the heart is automatically pumped without delay into the aorta and flows again through the circulation”. Based on this statement, cardiac output will be set equal to cardiac uptake, so that $Q_{HI} = Q_{OH}$. It is further noted in [11] that “.. the normal heart, functioning without any special stimulation, can pump an amount of venous return up to 2.5 times the normal venous return before the heart becomes the limiting factor ..” Therefore, a venous return function R is defined that incorporates all of the flow into the central venous compartment

$$R = Q_{YO} + Q_{GO} + Z_{JO}(P_J - P_O) + Z_{TO}(P_T - P_O) \\ + Z_{SO}(P_S - P_O) + Z_{XO}(P_X - P_O). \quad (129)$$

The cardiac uptake Q_{OH} is now defined in terms of this venous return and two regulatory multipliers $SNSo$ and OVP by

$$Q_{OH} = SNSo(P'_I) \cdot OVP(P_O) \cdot R \quad (130)$$

where P'_I denotes the time derivative of the arterial pressure function P_I . Since $Q_{HI} = Q_{OH}$, cardiac output is now based on the venous return through equation (130).

The multiplier $SNSo$ in (130) is associated with cardiac regulation by the sympathetic nervous system (SNS). It models an SNS mechanism that increases or decreases the heart rate in response to a change in arterial pressure. As noted in [11], a decrease in arterial pressure can markedly increase heart activity, with the heart rate increasing to as high as 160–180 bpm from the normal value of 72 bpm. A linear model for the $SNSo$ multiplier as a function of the instantaneous time derivative P'_I is

$$SNSo(P'_I) = 1 - \frac{P'_I}{10}. \tag{131}$$

This relationship produces an increase in heart rate to about twice the normal level as the result of a pressure drop of 20 mmHg. Note that $SNSo(0) = 1$, so that this regulatory mechanism is only active when P_I is changing.

The OVP function in equation (130) insures that if venous pressure drops, then so does cardiac uptake. It corresponds to the cardiac output versus right atrial pressure curve in [11] and is defined by

$$OVP(P_O) = \frac{M}{1 + (M - 1)e^{r(\bar{P}_O - P_O)}} \quad \text{where } M = 2.5 \text{ and } r = 0.5. \tag{132}$$

Since $OVP(\bar{P}_O) = 1$, this regulatory mechanism is not active when central venous pressure remains at its mean value.

Using the above cardiac forcing terms leads to a system of equations that describe mean pressures in the sense that the oscillations that occur about a mean pressure value are removed and the mean pressure may be considered a temporal average over one cardiac cycle. However, when trying to resolve circulatory pressure pulsations caused by cardiac output, a more instantaneous description of cardiac output is necessary. For this purpose, the cardiac function utilized in the present model is that described in [37]. Again in this case, cardiac output is set equal to cardiac uptake.

2.4. Model validation tests and applications to pathology

To validate the present whole-body model for intracranial pressure dynamics, several types of simulations assuming normal physiology were carried out and the results compared to clinical observations. In the first type of simulation, a pulsatile form for cardiac output was introduced as forcing so that the model's predicted pressure responses could be compared to clinically measured pressure pulsations in healthy humans. The pulsatile cardiac output function described in [37] (with parameter values $n = 11$, $\phi = .27882$, and $\sigma = 5.958$) was used as the cardiac forcing function (Q_{HI}) in the model's governing equations. This function is depicted in Figure 4 and represents the cardiac output over two cycles. A similar curve for the cardiac output of a dog has been given in [11]. A mean value for central artery pressure of 96 mmHg was prescribed as an initial condition for the first simulation. In the second type of simulation, a constant flow infusion test was used to validate the model's representations for variable intracranial compliances and intracranial fluid dynamics. In these simulations, the governing equation for

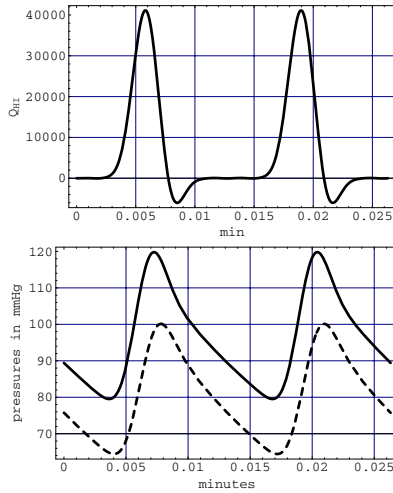


Fig. 4. The pulsatile cardiac forcing in ml/min (top), the 120/80 central artery pressure response (solid curve, bottom) and the 100/65 intracranial artery pressure response (dashed curve, bottom).

the extra-ventricular CSF compartment (T) was augmented by adding a constant infusion term to model the clinical infusion of mock CSF into the lower lumbar space.

With the lower body region explicitly represented by separate compartments in the present model, the effect of orthostatic forces on cerebral blood flow as the body changes position can be considered. Two additional types of simulations were now run to validate the modeling of the regulatory mechanisms associated with the systemic nervous system. The normal physiology value for the resistance R_{XO} was increased twofold and R_{IZ} was decreased by one half to simulate a change in body position from lying down to standing up, and the behavior of the cerebral blood flow Q_{AC} was then examined. These resistance changes were made instantaneously and the modeled effect on cerebral blood flow was determined for the next 30 seconds. In the first simulation of this type, the model equations included all of the SNS reflexes described in Sections 2.3.3 and 2.3.4. In the second simulation, the SNS terms were removed from the governing equations.

To examine the potential predictive capabilities of the model in pathological conditions, simulations were run where all cardiac forcing in the model was suddenly stopped to simulate cardiac arrest, i.e. Q_{Hi} and Q_{OH} were suddenly set equal to zero. A blood volume of 5600 ml was assumed in these simulations, and the response of pressures in the model's circulatory compartments was determined. This behavior, and the predicted final circulatory compartmental pressure values, were then compared to clinical results associated with cardiac arrest and the filling pressure of the circulation.

As a second example of pathology, simulations of hemorrhagic shock were carried out. Hemorrhage was modelled by the inclusion of an outflow path, denoted

Q_{XM} , from the lower venous compartment (X) into the ambient atmosphere (M). This flow was calculated so as to achieve a 45% loss in blood volume at the end of the simulation. The percent changes in central artery pressure, cardiac output, and cerebral blood flow were then calculated with respect to percent blood loss.

In all of these simulations, the model's system of differential equations was solved numerically using the symbolic mathematical software package *Mathematica* employing maximum accuracy settings. Specifically, the program NDSolve was used for this task. It was determined that increasing the AccuracyGoal or PrecisionGoal options in this program did not change the results from the default setting.

3. Results

3.1. The pulsatile forcing simulation

The usual systolic and diastolic values of pulsatile central artery pressure are perhaps the best-known values in human physiology. Figure 4 shows the behavior of central artery pressure predicted by the present model in response to the pulsatile cardiac forcing developed in [37]. The model's predicted response to a mean value of 96 mmHg, prescribed as an initial condition, reproduces a peak systolic pressure of 120 mmHg and a diastolic pressure of 80 mmHg. Figure 4 also depicts the intracranial artery pressure response. Here, the predicted systolic and diastolic pressures are "100 over 65." These values are typical of those in the small arteries [11].

3.2. The CSF infusion simulation

The results of these simulations are depicted in Figure 5.

3.2.1. The CSF pressure-volume relation

The pressure-volume relation obtained by using the present model to simulate CSF infusion tests is given in Figure 5. The pressure in this figure is the pressure P_T of the extra-ventricular CSF compartment since this compartment contains the lower lumbar portion of CSF space where clinical pressure recordings were made. The volume change in Figure 5 represents the net change of both ventricular and extra-ventricular CSF volumes combined, as this is the quantity calculated in the experiments. The logistic-like shape of the predicted pressure-volume relationship is maintained until CSF pressures reach high values comparable to the systolic blood pressure. At this point, the curve turns upward and compliance rapidly decreases.

3.2.2. The conductance of CSF outflow

The same infusion simulations that led to the pressure-volume relationship in Figure 5 may also be used to calculate a relationship between CSF pressure increases and CSF absorption. The slope of this relationship is known as the conductance of CSF outflow and is denoted by C_{out} . In model simulations, this value is easily calculated by

$$C_{out}^m(t) = \frac{Z_{TS}(P_T(t) - P_S(t)) + Z_{TO}(P_T(t) - P_O(t)) - (\bar{Q}_{TS} + \bar{Q}_{TO})}{P_T(t) - \bar{P}_T} \quad (133)$$

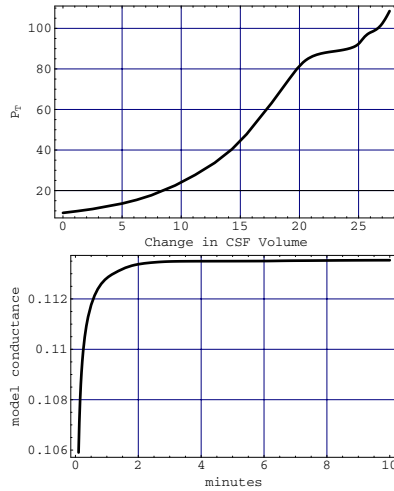


Fig. 5. The predicted CSF pressure/volume curve (top) and the model conductance to CSF output (bottom).

where the superscript m denotes the model calculation and t denotes the time in minutes from the start of the simulated infusion. The bottom plot in Figure 5 displays the predicted conductance of CSF outflow throughout ten minutes of an infusion simulation.

3.3. Position change and cerebral blood flow

Figure 6 depicts the results of modifying the resistances between the central and lower body in the model to simulate a change in body position from lying down to standing up. The solid curve in Figure 6 indicates the response of cerebral blood flow to this change in position with the SNS reflexes included in the model equations. The simulation predicts that with all SNS reflexes activated, cerebral blood flow is maintained at 100% by the model through the change in body position. The dashed curve in Figure 6 shows the predicted behavior of cerebral blood flow in the absence of regulation by the SNS. In this case, the change in position results in a reduced cerebral blood flow that tends to approximately 94% of its prior value.

3.4. Cardiac arrest and mean filling pressure

In this simplified simulation of cardiac arrest, when all cardiac forcing is stopped by setting $Q_{OH} = Q_{HI} = 0$, a rapid equilibration of compartmental pressures occurs. All circulatory pressures in the simulation tend to 7.5 mmHg after approximately 45 seconds.

3.5. Hemorrhage

The results of these simulations are depicted in Figures 7 and 8.

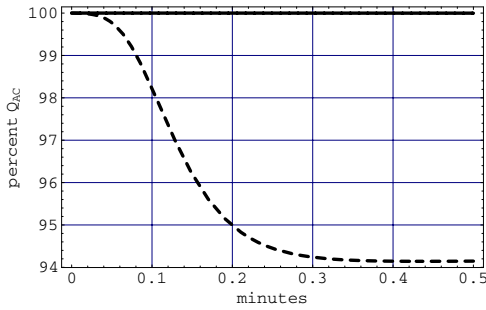


Fig. 6. Percentage of Q_{AC} drop due to a positional change with all SNS reflexes activated (solid curve), and without any SNS reflexes included (dashed curve).

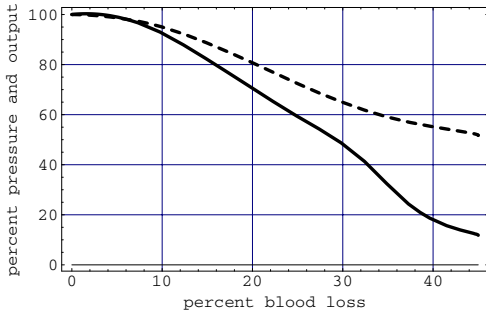


Fig. 7. Percentage decrease of \bar{P}_I (dashed curve) and of \bar{Q}_{HI} (solid curve) as a function of percentage blood loss due to hemorrhage.

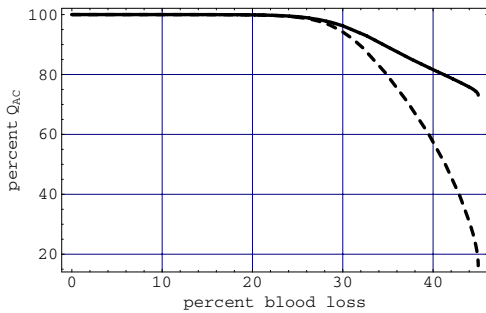


Fig. 8. Predicted percentage of Q_{AC} drop versus percentage of blood loss due to hemorrhage with both SNSz reflexes activated (solid curve) and no SNSz reflexes included (dashed curve).

3.5.1. Arterial pressure and cardiac output

Figure 7 gives the predicted percentage drop in central artery pressure (P_I) and cardiac output (Q_{HI}) with respect to percent blood loss as a result of a simulated hemorrhage from the lower venous compartment. In the results of this simulation, the predicted arterial pressure and cardiac output remain very stable over the first

10% blood loss and the relative arterial pressure stays above relative cardiac output during the course of the hemorrhage. Beyond a 30% blood loss, a second plateau occurs in the arterial pressure curve. The central venous compartment contracts to less than 50% of its original volume during the simulated hemorrhage. However, neither arterial pressure nor cardiac output have dropped to zero by the end of the simulation when a 45% blood loss has occurred.

3.5.2. Cerebral blood flow

Figure 8 depicts the predicted percentage drop in cerebral blood flow (Q_{AC}) with respect to percent blood loss during the simulated hemorrhage. The solid curve represents results when both SNSz mechanisms in Section 2.3.3 are intact, and the dashed curve represents results when both SNSz mechanisms are disabled. Both simulations predict that a 25% blood loss can be tolerated without a significant reduction in cerebral blood flow. Above this degree of blood loss, with the SNS mechanisms intact, the blood supply to the brain remains above 75% of its original value. However, without these SNS regulatory mechanisms included in the model's equations, cerebral blood flow drops quickly to 20% its original value.

4. Discussion

Lumped-parameter compartmental models of the present type have a long history, dating to the earliest such model of the intracranial system formulated by Monro in 1783 [25]. This first model was bi-compartmental, considering incompressible brain matter and blood as its two constituents. In the work of Monro's student Kellie [18] 40 years later, the vascular compartment was further subdivided into arterial and venous blood to produce a three compartment model. Since the pioneering work of Monroe and Kellie, increasingly more complex models of the intracranial compartment have been posited in order to more realistically describe the relationship between intracranial pressures and volumes. There has been a steady increase in the number of fluid compartments, the introduction of a separate cerebrospinal fluid compartment, the inclusion of cardiovascular input, and a relaxation of the treatment of system constituents as incompressible fluids and matter [2, 3, 6, 12, 16, 17, 22, 23, 33, 35]. As noted by Agarwal *et al.* [3], the intracranial system involves a number of subsystems which interact through complex mechanisms, and the classical piecewise approach, which often considers CSF dynamics separately, is not suited to studying multiple parameter changes and the effects of interconnected subsystems on each other. By contrast, lumped-parameter models of the intracranial system are capable of including and linking different subsystems, so that such interactions can be examined.

When considering lumped parameter models, it is important to realize that a compartment does not necessarily correspond to a precise physical location in the body. For example, with a single CSF compartment in a model, CSF in the ventricles cannot be distinguished from CSF in the subarachnoid and spinal spaces. This is one of the main limitations of the lumped-parameter approach. Additional spatial resolution can be realized only by subdividing the physical system into a larger number of compartments based on spatial considerations. For example, distinct ventricular CSF and extra-ventricular CSF compartments may be included as

opposed to a single lumped CSF compartment. In principle, the entire body could be finely subdivided in this manner into separate compartments to provide the desired degree of spatial resolution. However, clearly this subdivision process cannot be carried to an extreme as the resulting system of linked governing equations will rapidly become too large for practical analysis and solution.

Despite their evolving complexity, two common features characterize most earlier lumped-parameter models for pressure dynamics in the intracranial system. The first common feature is an assumption that all resistance and compliance parameters can be represented by constants. This leads to a linear system of governing differential equations. The second common feature is adoption of the “Kellie-Monro Doctrine,” which assumes that the intracranial system can be confined within the cranial vault. By requiring that inflow to the intracranial arteries equals outflow from the jugular bulb, this assumption produces a closed system that conserves total intracranial volume.

The use of linear equations can be expected to be valid provided the allowable range of pressure variations is suitably limited. However, even for these restricted situations, important physical features of the intracranial system must be omitted. In the case of resistances, which relate pressure differences and flows, assuming constant values allows, at best, cerebrovascular autoregulation by indirect means. In the case of compliances, which relate pressures and volume changes, constant values imply that the same pressure gradients between adjacent compartments will always produce the same volume changes, independent of the base pressure levels themselves, and without a bounding mechanism.

Exceptions to the trend assuming constant parameters include the work of Agarwal *et al.* [3], Hoffmann [13], Lakin *et al.* [20], Kadas *et al.* [15], and Stevens and Lakin [38]. In the mathematical model of Agarwal *et al.* [3], which is presented in terms of hydraulic and electrical analogies, constant resistance to flow is assumed at the outflow of a compartment. However, capacitance values are nonlinear functions of transmural pressures. The mathematical model formulated by Hoffmann [13] to analyze the CSF and hemodynamics of the intracranial system is not, strictly speaking, a lumped-parameter compartmental model. However, it does consider intracranial space as a rigid container filled with brain tissue, CSF, and blood in the arterial and venous portions of the cerebral vascular bed. Autoregulation is included in the model with the aid of a variable flow resistance located in a vessel, representing the small arteries, arterioles, and capillaries, which connects the arterial and venous sides of the vascular bed. However, the variable nature of the flow resistance is not preserved in [13] beyond the development stage since, to allow determination of closed form solutions when examining the intracranial pulse pressure relationship and hemodynamics, the flow resistance is assumed to be constant over a cardiac cycle. In the lumped-parameter model of Kadas *et al.* [15], a true variable resistance dependent on the pressure difference between the intracranial arteries and capillaries is used to achieve autoregulation of cerebrovascular flow at the arteriole-capillary interface.

Lakin *et al.* [21], extend an earlier seven-compartment model first described by Karni *et al.* [17] then elaborated by Sorek *et al.* [35] and consistently reformulate their model to deal with the overdetermined nature of the system. A key feature

in [21] is the introduction of a non-constant compliance between the CSF and brain matter compartments. The form chosen for this pressure-difference dependent compliance is motivated by the success of a logistic model developed by Lakin and Gross [19] for the global intracranial pressure-volume relationship. The use of a logistic expression for the pressure-dependent compliance C_{FB} between the brain matter compartment and single CSF compartment in the seven-compartment model has been validated through a comparison of this model's predictions for the response to CSF bolus manipulation with corresponding experimental data obtained in the rabbit [20]. The concept of variable compliances between compartments has been further extended by Stevens and Lakin [38]. In this work, more general pressure-difference dependent compliances involving exponentials and multiple parameters are developed, calibrated, and validated through simulated steady-state infusion tests.

When the intracranial space is treated as a closed volume-conserving system contained within the (nearly) rigid cranial vault, important mechanisms for the influence of extracranial physiology on intracranial pressure dynamics cannot be included in the resulting models. For example, the ability of the spinal portion of CSF space to buffer fluctuations of intracranial CSF pressures cannot be directly introduced under the Kellie-Monro Doctrine.

Two previous mathematical models of intracranial pressure dynamics include aspects of extracranial physiology. The first model, formulated by Czosnyka *et al.* [8,9], includes a compliance for CSF storage within the lumbar channel. This model contains three compliances, four resistances, and involves differential equations based on a hydrodynamic model for the physical system and its electrical circuit equivalent. It allows the dynamic relationship between cerebral perfusion pressure, intracranial pressure, and cerebral blood flow in various states of autoregulation to be studied [8]. Use of this model in conjunction with clinical data [9] has determined which of the indices that can be derived using transcranial Doppler ultrasonography and trends of intracranial pressure and blood pressure are useful in clinical tests of autoregulatory reserve.

The second model, due to Stevens and Lakin [38], uses a single ground compartment to represent the portion of the body below the clavicles. This model contains three resistances, including a resistance between the intracranial veins and the rest-of-body compartments. Thus, outflow from the intracranial system depends on pressure differences and need not instantaneously equal the specified inflow. The model also contains three compliances, including a compliance between the CSF and rest-of-body compartment that represents the ability of the spinal portion of CSF space to expand and buffer CSF pressures by compressing the large veins that surround the spinal theca. Two of the three model compliances are pressure dependent. As has been noted, use of some variable compliances in lumped-parameter models is essential to accurately represent intracranial pressure dynamics. This work demonstrates how the multiple model compliances C_{ij} that relate local volume adjustments between adjacent compartments in lumped-parameter models can be consistently related to the single experimentally-determined global compliance C_g between the entire CSF system (including extracranial portions) and the rest of the body. The link established between the model parameters and this physical parameter is validated by using model simulations to recover the measured CSF

pressure-volume relationship given in [39]. The associated functional forms for the pressure-dependent compliances determined in [38] are used in the present work.

The current lumped-parameter model for pressure dynamics embeds the intracranial system in extensive whole-body physiology. It includes 16 distinct body compartments. Of these compartments, 8 lie entirely outside of the cranial vault. An additional compartment containing extra-ventricular CSF lies partially outside of the cranial vault and includes both the subarachnoid and spinal portions of CSF space. This bridging compartment explicitly allows for buffering of CSF pressures by the spinal theca.

The physical constituents in subunits of the present model are blood, CSF, and tissue and interstitial fluid. With the single exception noted below, each compartment is composed of a single constituent. Spatial resolution is obtained by first dividing the body into intracranial and extracranial components. The body's extracranial physiology is subdivided into a lower region below the pelvis and a central portion that includes the region between the pelvis and the clavicles as well as the extracranial portions of the body above the clavicles. The vascular system in each of these three regions is divided into separate artery, capillary, and vein compartments. However, in the intracranial space, the choroid plexus capillaries are placed in a separate compartment from the rest of the intracranial capillary bed. This allows these capillaries to autoregulate to maintain the production of CSF when ventricular CSF pressures rise or fall. The venous-sinus veins where CSF absorption occurs through the arachnoid villa and the jugular veins are also placed in a compartment separate from the remainder of the intracranial veins. The CSF space is divided into two compartments containing ventricular and extra-ventricular CSF. Two of the three regions contain a separate compartment for the tissue and interstitial fluid. The exception is the central region where the tissues, organs (except for the heart), and pulmonary circulation are lumped into a composite rest-of-body compartment. The central region contains an explicit representation for the heart pump, and a realistic pulsatile cardiac output [37] provides the major forcing in the current model. The cardiac output function used in the present simulations is depicted in Figure 4 and is based on a mean cardiac output of 6900 ml and a heart rate of 76 beats per minute.

The model also allows for interaction with the external environment through flows representing the ingestion and elimination of fluid via the central body. Consequently, beyond the 16 compartments that contain body matter, the external environment is considered an implicit 17-th compartment in this model. Terms involving any time variations of ambient atmospheric pressure appear in the governing equations, and two compliances allow the volume of the body to adjust relative to the ambient environment.

In addition to allowing direct flows (e.g. arteries to capillaries to veins) between adjacent compartments, the present model includes the transfer of fluid between capillaries and tissue by filtration. These flows are governed by the Starling-Landis equation and are driven by differences between the colloid osmotic pressures of the blood plasma in the capillaries and the interstitial fluid as well as by the usual compartmental pressure differences between capillaries and tissue. Filtration mechanisms are included between the capillaries and tissue compartments in the central

and lower portions of the body in the present model. In the intracranial region, significant colloid osmotic pressure differences do occur between the intracranial capillary and tissues. However, the endothelial cells that make up the intracranial capillary wall are so tightly joined that not even water molecules can usually pass between them [32]. Thus, under normal conditions, colloid osmotic pressure forces in the intracranial region are irrelevant. In the case of highly elevated capillary pressure it is possible for the intracranial capillary wall to expand enough to allow water molecules to pass between the endothelial cells, and at this point both colloid osmotic pressures and regular pressures start governing filtration rates. At these elevated pressures, the description of intracranial capillary filtration as a function of capillary pressure will clearly be nonlinear. However, to simplify the equation for intracranial filtration, this relationship may still be linearly approximated with the slope defined by Z_{CB} , Z_{BV} , and Z_{FB} .

A lymphatic system is also included in the present model. This system allows interstitial fluid in the tissue compartments of the central and lower regions of the body to flow directly into the central venous compartment. Lymphatic flows are thus able to balance filtration in these regions and establish an equilibrium state. Lymphatic flow is not introduced in the intracranial region as the brain appears to lack lymphatic vessels. However, drainage of interstitial fluid via the Virchow-Robins Spaces is accommodated by pathways between the Brain and CSF compartments.

In all, the present model contains 16 compliance parameters, of which 8 are variable and depend on pressure differences. There are also 23 resistance parameters. Four intracranial resistances are pressure-dependent and autoregulate flow to both the cerebral capillary bed and the choroid plexus as well as the production of CSF in the choroid plexus. CSF production is known to be nearly constant over a wide range of pressures. However, the production of CSF decreases when perfusion pressure decreases to low values [39], and a mechanism that ramps down CSF production when perfusion pressure falls below 55 mmHg is also included in the model.

The present model also includes a group of regulatory mechanisms associated with the sympathetic nervous system (SNS). Two variable resistances in the central and lower regions provide for SNS regulation of arterial pressure through constriction of the arterioles. Included in these variable resistances is the dramatic “last ditch stand” [11] triggered by the SNS when arterial pressure falls to a level where cerebral blood flow is affected. The far less extreme SNS regulation of arterial pressure through a constriction of the large vascular vessels in the central body is also represented in the model. Active interfaces are placed between the central rest-of-body compartment and the central artery and vein compartments. When arterial pressure falls, forcing terms in the governing equations for compartments Y, I, and O force the volume cups at the active Y-I and Y-O interfaces into the vascular compartments, providing the regulatory constriction. An additional SNS mechanism in the model regulates central arterial pressure by increasing the number of heartbeats per minute if arterial pressure falls.

The heart pump provides the primary forcing for the model’s coupled differential equations. This pump is divided into the Right Heart and Left Heart in the present model. Cardiac uptake in the model is defined in terms of the venous re-

turn. In addition to the factor noted above through which the SNS modifies cardiac activity, the model's expression for cardiac uptake also includes a factor that insures cardiac uptake will fall if venous pressure drops. Cardiac output from the Left Heart is assumed equal to the cardiac uptake by the Right Heart, so that $Q_{HI} = Q_{OH}$. This produces a conservation of total heart volume. However, it also reflects physiology that maintains a constant pulmonary circulation volume with cardiac output to the pulmonary arteries balanced by cardiac uptake from the pulmonary veins. In this situation, the pulmonary circulation can be removed as a separate component of the system and may be consistently lumped into the model's composite compartment Y.

Calibration of scale values for all resistance and compliance parameters from available physical data and other relationships must be accomplished before the model's governing differential equations can be used in simulations. A key step in calibrating model compliances is determining the distensibilities of the extracranial compartments of the model. In particular, each extra-cranial compartment has an associated total compliance equal to the product of its associated volume and distensibility. It should be noted that calculating compliances by this technique yields a total central artery compliance $C_I = 1.529$ ml/mmHg, which is within 5 percent of the data value of 1.445 ml/mmHg for total arterial compliance measured in the ascending aorta by Chemla *et al.* [5]. The central venous compliance calculated by these methods yields $C_V = 50$ ml/mmHg while the graph depicting the systemic venous pressure volume curve in [11] suggests a total venous compliance of 50 ml/mmHg. Finally, Noordergraaf [29] states that the systemic arterial compliance is between 1 and 2 ml/mmHg and systemic venous is between 50 and 200 ml/mmHg, where the 50 ml/mmHg comes from [11]. Clearly the values calculated by the present procedure all fall within these ranges.

Because even the most complex mathematical model must be based on assumptions and simplifications of actual physiology, model validation is an essential step in the development process. In the present case, after calibration of parameters associated with healthy human physiology, the model was used in two types of simulations and the results compared to physical data. In the first type of simulation, the response of compartmental pressures to the realistic pulsatile cardiac output [37] given in Figure 4 was determined. As also shown in Figure 4 the predicted response of central arterial pressure is the typical "120 over 80" blood pressure readings expected in healthy humans. Furthermore, the wave form and magnitudes of this pressure response match well with those described in [11]. It is worth noting that a mild incisura (dicrotic notch) is discernable in this pressure curve. This notch is typical in central artery pressure readings, although it is usually more pronounced than in Figure 4. In particular, the present model cannot capture reflected waves which have a tendency to cause a second (usually higher) systolic peak and hence a more prominent inflection point.

The response of the intracranial arteries is also shown in Figure 4. This response agrees well with the estimates given in [11] for pressure pulses in the small arteries. The pressure responses of other intracranial compartments were also within expected ranges.

Constant flow infusion tests were also simulated using the present model. These tests have been described in [4,10] and elaborated upon by [39]. In these experiments, mock CSF was infused at a constant rate into the lower lumbar space. The pressure of this space was then measured and associated with a calculated total CSF volume change. This resulted in determination of a curve known as the global pressure-volume relation. The slope of this curve describes the elastance of the entire CSF space, including extracranial portions. The inverse of the elastance is the more well-know compliance.

The typical clinical global CSF pressure-volume relation, except at extreme pressures, is an S-shaped curve of logistic type. It has a lower pressure plateau near resting pressure, defined as the pressure where CSF production in the system is just balanced by CSF absorption by the venous system [39]. This region of small slope (large compliance) is due to the ability of the system to easily accommodate increases in the volume of the CSF space at these relatively low pressures through the compression of the venous system. As additional CSF volume is added to the system and pressures increase, this capacity for adjustment diminishes as there will be less venous blood available to eject to further compress the veins. Thus, with increasing pressures, the pressure-volume curve steepens indicating a reduction in the compliance of the system. The slope of the pressure-volume relationship continues to increase for larger infusion volumes until the resulting CSF pressures are high enough that the intracranial arteries can begin to be compressed. At this point, some additional compliance enters the system. There is a point of inflection in the curve followed by a region of decreasing slope that leads to an upper pressure plateau at the diastolic pressure of the intracranial arteries. Once additional volume increases beyond this point increase CSF pressures to the systolic pressure of the intracranial arteries, there are no additional mechanisms available to buffer additional volume increases, and the compliance of the CSF system falls to zero.

To model the experimental introduction of mock CSF into the lower spinal space, a source term for mock CSF was added to the governing equation for the model's extraventricular CSF compartment. Simulations were then run in which a given volume of mock CSF was introduced into this compartment, and the pressure responses of the body were determined. A global pressure-volume relationship was then formed based on the simulation results. As indicated in Figure 5, this simulated pressure-volume curve captures all of the relevant aspects of the clinically observed relationship, including the rapid decline in compliance when CSF pressures are above systolic artery pressure.

This same group of infusion simulations was also used to calculate a relationship between CSF pressure differences and CSF absorption. The slope of this relationship is known as the conductance C_{out} of CSF outflow. When C_{out} has been studied experimentally [4], a linear relationship between CSF pressure increase and CSF absorption is observed. In [4], a mean value for C_{out} of 0.11 (ml/min)/mmHg is given for a sample of eight healthy volunteers, and it is stated in [39] that a value greater than 0.10 is probably normal. The values of the conductance of CSF outflow calculated from the present simulations are shown in Figure 5. These values change with time, but stay within .004 units of the mean value of 0.11 (ml/min)/mmHg in [4]. They are also greater than 0.10 as suggested by [39]. Furthermore, the calcu-

lated temporal variation of C_{out}^m is sufficiently small that the relationship between CSF pressure increase and CSF absorption might easily be categorized as linear on the basis of clinical data.

In the current model calibrations, the pressures, flows and hence resistances are determined from data associated with the body being in the horizontal (supine) position. Gravitational influences on the circulation will change when the body changes position. Upon standing up, the blood flow into the lower body is aided by gravity, but the venous return from the lower body is hindered by it. As the lower body in the present model is represented by separate compartments, the effect of a positional change can be considered. To simulate the gravity-induced changes associated with standing up, the resistance into the lower arteries (R_{IZ}) may be decreased by one half while the resistance from the lower veins (R_{XO}) is doubled. This results in pressure and volume increases of the lower arteries and veins. In the current simulations, these resistance changes were made instantaneously and the modelled effect on cerebral blood flow was determined for the next 30 seconds. In the first simulation, all sympathetic nervous system (SNS) reflexes are intact and in the second these are removed. As can be seen in Figure 6, with all SNS reflexes activated, cerebral blood flow is maintained at 100% of its original value.

When the SNS reflexes are removed from the model equations, cerebral blood flow drops to about 94% of its original value due to the positional change. This predicted decrease indicates the important role that the SNS regulatory mechanisms play in the maintenance of cerebral blood flow in the model. The decrease also confirms that loss of the SNS reflexes can be a factor in orthostatic intolerance. Syncope, or fainting, is a common event with many different causes. Syncope can be due to sudden vasodilatation (vasodepressor or “vasovagal” syncope) as well as postural hypotension, in which the normal vasoconstrictive reflex response to a transiently decreased cardiac output on standing is not sufficiently active. Postural hypotension can occur as the result of drugs, venous disease, sympathectomy, hypovolemia, peripheral neuropathy, in addition to degeneration of the sympathetic nervous system (primary autonomic insufficiency, or idiopathic orthostatic hypotension). Common to all causes of syncope is a decrease in cerebral blood flow to under 30 ml per 100 g brain tissue per minute from the usual 50-55 ml, about 55% of normal [1]. This is well above the threshold for loss of electrical function, at 30% of normal [14], but is enough to cause a transient loss of consciousness. The calculated percentage decrease in cerebral blood flow in the current simulation with the SNS terms in the model equations omitted does not approach the levels associated with fainting due to a rapid change in position as the result of standing up too quickly, even with inactive SNS reflexes. However, cerebrovascular autoregulation in the current simulation remains uncompromised and will act to maintain cerebral blood flow despite sudden decreases in arterial pressure.

To demonstrate the potential predictive capabilities of the model in pathology, two situations were simulated. In the first of these, a simplified representation of cardiac arrest was created by suddenly terminating all cardiac forcing, i.e. setting $Q_{HI} = Q_{OH} = 0$, at a specified time in the course of the simulation. Gutyon [11] notes that “When heart pumping is stopped ... the flow of blood everywhere in the circulation ceases a few seconds later. Without blood flow, the pressures everywhere

in the circulation become equal after a minute or so. This equilibrated pressure level is called the *mean circulatory filling pressure*... at a volume of 5000 ml, the filling pressure is the normal value of 7 mmHg.” Predicted results from the simulation were consistent with this statement. When all cardiac forcing was stopped in the simulation, all circulatory pressures tend to 7.5 mmHg after about 45 seconds. The small difference in the predicted and cited filling pressures may be partially due to the fact that, consistent with [24], total blood volume in the simulation was taken to be 5600 ml rather than the 5000 ml in [11].

The second pathological situation considered as a test of the model’s capabilities involves the effects of shock caused by hypovolemia. In these simulations, a flow term Q_{XM} was introduced into the equation for compartment X to model a hemorrhage from the lower body. Guyton [11] gives a clinically-derived graph that, as in Figure 7, depicts the percentage drop in central artery pressure (P_I) and cardiac output (Q_{HI}) with respect to percent blood loss. Consistent with these clinical results, the modeled response shows very stable pressure and cardiac output over the first 10% blood loss, and the relative arterial pressure stays above relative output during the entire course of the hemorrhage. At 30% blood loss, the relative drops in pressure and cardiac output are also in close agreement with the clinical results. During the course of the simulated hemorrhage, the central venous compartment contracts to less than 50% of its original volume, indicating that the active interface (SNSc) in the model is causing the central veins to strongly constrict in order to maintain blood flow back to the heart. Beyond 30% blood loss, a second arterial plateau is noticed in Figure 7. This important feature, which is also noted in the clinical results, is due to the “last-ditch stand” reflex to maintain blood supply to the brain provided by the regulatory multiplier $SNSz(Q_{AC})$ in equation (130). At about 45% blood loss, clinical results show both pressure and cardiac output dropping quickly to zero. As indicated in Figure 7, this behavior was not reproduced in the simulation. When central artery pressures fall even briefly below a critical level, a hemorrhagic shock becomes self-reinforcing due to degeneration of the circulatory system, including changes in the heart’s muscle cells. The present model is incapable of representing the multiple degenerative components of a progressive shock, and thus predicted values of central artery pressure and cardiac output beyond a 40% blood loss in Figure 7 come from using the model beyond its expected range of applicability.

The role of the SNS regulatory mechanisms in maintaining adequate central artery pressure and cardiac output has been noted above. However, the need to include the arteriole constrictive reflex $SNSz$ in a model of intracranial pressure dynamics when simulating pathology is also dramatically illustrated by the behavior of cerebral blood flow as a function of blood loss in the hemorrhage simulations. Due to the intracranial autoregulatory mechanism Z_{AC} in the model, a 25% blood loss can be tolerated without significant reduction in cerebral blood flow. Beyond this point, arteriole constriction is essential to further maintain adequate levels of cerebral blood flow. As indicated in Figure 8, predicted cerebral blood flow Q_{AC} remains above 80% of its original value from a 25% blood loss through a 40% blood loss. By contrast, in an analogous simulation where the arteriole constrictive response was disabled, Q_{AC} falls to approximately 55% of its original value when

a 40% blood loss has occurred. Between a 40% and 45% blood loss, Q_{AC} remains above 75% of its original value with the arteriole constrictive response intact, but falls rapidly from 55% to approximately 20% of its original value with the arteriole constrictive response disabled. As noted above, the model does not include the circulatory failure associated with progressive shock that occurs with this degree of blood loss, so the simulation results in the 40% to 45% blood loss range will upper bounds on actual expected values. Nevertheless, the dramatic effect of the “last-ditch stand” response in maintaining cerebral blood flow in the model is clear.

5. Conclusions

This work has shown that a mathematical model for intracranial pressure dynamics can be formulated which consistently embeds the intracranial system within extensive whole-body physiology. The current model thus fully revokes the “Kellie-Monro Doctrine” that has previously restricted lumped-parameter models of the intracranial system. With the lumped-parameter approach, 16 separate body compartments are required in the present model to achieve adequate spatial resolution. Variable compliances and resistances must be used within the intracranial space to realistically provide for cerebrovascular autoregulation, regulation of CSF production, and the volume adjustments produced by changing pressure differences. With extracranial physiology now an integral part of the model, flows involving filtration between the capillaries and tissues, lymphatic flows, and the regulation of arterial pressure and cardiac activity by the sympathetic nervous system must be included. Particular care must also be taken in descriptions of the cardiac uptake and output. The resulting nonlinear mathematical model is far more complex than in previous work, and calibration of the numerous model parameters from experimental data and derived relationships introduces significant overhead into use of this model for simulations. However, validation tests show that the model’s predictions are in excellent agreement with experimental data for normal physiology. Additional simulations indicate that the present whole-body model appears to have significant potential predictive capabilities in situations involving pathological conditions.

Acknowledgements. Portions of this work were supported by the National Science Foundation under grant number DMS-96-26391 and by NASA under grant number NGT5-40110 and cooperative agreement number NCC5-581. We also wish to acknowledge the contributions to this work of our colleague and friend, Dr. Cordell Gross. The untimely death of Dr. Gross toward the start of this work was a great loss to Neuroscience.

References

1. Adams, R.D., Victor, M.: Principles of Neurology (Second Edition). New York, McGraw Hill, 1981
2. Agarwal, G.C.: Fluid flow—a special case. In Brown JHV, Jacobs JE, Stark L, eds. Biomedical Engineering. Philadelphia, F.A. Davis, 69–81 (1971)
3. Agarwal, G.C., Berman, B.M., Stark, L.A.: A lumped parameter model of the cerebrospinal fluid system. IEE Trans Biomed Eng 45–53 (1969)
4. Albeck, M.J., Gjerris, F., Sorenson, P.S., *et al.*: Intracranial pressure and cerebrospinal fluid outflow conductance in healthy subjects. J Neurosurgery 74, 597–600 (1991)

5. Chemla, D., Herbert, J.L., Coirault, C., Zamani, K., Suard, I., Colin, P., LeCarpentier, Y.: Total arterial compliance estimated by stroke volume-to-aortic pulse pressure ratio in humans. *Am J Physiol* **274** (Heart Circ Physiol 43), 500–505 (1998)
6. Chopp, M., Portnoy, H.D.: Systems analysis of intracranial pressure. *J. Neurosurgery* **53**, 516–527 (1980)
7. Curreri, P.W.: Burns. In Schwarts S, Shires, Spenser Stoier, eds. *Principles of Surgery*, 3rd Ed. New York, McGraw Hill, 285–302 (1979)
8. Czosnyka, M., Piechnik, S., Koszewski, W., Laniewski, P., Maksymowicz, W., Paluszek, K., Smielewski, P., Zabolotny, W., Zaworski, W.: The dynamics of cerebral blood perfusion pressure and CSF circulation – a modelling study. In Avezaat *et al.* (eds.), *Intracranial Pressures VIII*. Berlin-Heidelberg, Springer, 699–706 (1993)
9. Czosnyka, M., Piechnik, S., Richards, S., Kirkpatrick, P., Smielewski, P., Pickard, J.D.: Contribution of mathematical modelling to the interpretation of bedside tests of cerebrovascular autoregulation. *J. Neurol Neurosurg Psychiatry* **63**, 721–731 (1997)
10. Friden, H., Ekstedt, J.: Volume/Pressure relationships of the cerebrospinal space in humans. *Neurosurgery* **4**, 351–366 (1983)
11. Guyton, A.C.: *Textbook of Medical Physiology* (Tenth Edition). Philadelphia, PA: W.B. Saunders Company, 2000
12. Hakim, S., Venegas, J.G., Burton, J.D.: The physics of the cranial cavity, hydrocephalus and normal pressure: Mechanical interpretation and mathematical models. *Surg Neurol* **5**, 187–210 (1976)
13. Hoffmann, O.: Biomathematics of intracranial CSF and haemodynamics. Simulation and analysis with the aid of a mathematical model. *Acta neurochir Suppl* **40**, 117–130 (1987)
14. Jennett, B., Teasdale, G.: *Management of Head Injuries*. Philadelphia, PA: F.A. Davis Co., 1981
15. Kadas, Z.M., Lakin, W.D., Yu, J., Penar, P.L.: A mathematical model of the intracranial system including autoregulation. *Neurological Research* **19**, 441–450 (1997)
16. Karni, Z., Bear, J., Sorek, S., Pinczewski, Z.: A quasi-steady state compartmental model of intracranial fluid dynamics. *Med Biol Engng Comput* **25**, 167–172 (1987)
17. Karni, Z., Ivan, L.P., Bear, J.: An outline of continuum modelling of brain tissue mechanics. *J Child Neuro* **1**, 119–125 (1986)
18. Kellie, G.: An account ..., with some reflections on the pathology of the brain. *Edinburgh Med Chir Soc Trans* **1**, 84–169 (1824)
19. Lakin, W.D., Gross, C.E.: A nonlinear haemodynamic model for the arterial pulsatile component of the intracranial pulse wave. *Neurol Res* **14**, 219–225 (1992)
20. Lakin, W.D., Yu, J., Penar, P.: Mathematical modeling of pressure dynamics in the intracranial system. *Nova Journal of Mathematics, Game Theory and Algebra* 5–2 (1996)
21. Lakin, W.D., Yu, J., Penar, P.: Analysis and validation of a mathematical model for intracranial pressure dynamics. *Mathematical and Computer Modelling of Dynamical Systems* **3**, 54–73 (1999)
22. Lewer, A.K., Bunt, E.A.: Dysfunction of the fluid mechanical cerebrospinal systems as revealed by stress/strain diagrams. *S Afr Mech Eng* **28**, 159–166 (1978)
23. Miller, J.D.: Volume and pressure in the craniospinal axis. *Clin Neurosurg* **22**, 76–105 (1975)
24. Milnor, W.R.: *Hemodynamics* (Second Edition). Baltimore: Williams and Wilkins, 1989
25. Monro, J.: *Observations on the Structure and Functions of the Nervous System*. Edinburgh: W. Creech, 1783

26. Murgo, J.P., Westerhof, N., Giolma, J.P., Altobelli, S.A.: Aortic input impedance in normal man: relationship to pressure wave forms. *Circulation* **62**, 105–115 (1980)
27. Nichols, W.W., O'Rourke, M.F.: *McDonald's Blood Flow in Arteries: Theoretical, experimental and clinical principles* (Fourth Edition). New York: Arnold, 1998
28. Nylin, G., Hedlund, S., Regnstrom, O.: Studies of the cerebral circulation with labeled erythrocytes in healthy man. *Circ Res* **9**, 664–674 (1961)
29. Noordergraaf, A.: *Circulatory System Dynamics*. New York: Academic Press, 1978
30. Osborne, A.G.: *Introduction to cerebral Angiography*. Hagerstown, Harper and Row, 379–428 (1980)
31. Parazynski, S.E., Hargens, A.R., Tucker, B., Aratow, M., Styf, J., Crenshaw, A.: Transcapillary fluid shifts in the tissues of the head and neck during and after simulated microgravity. *J. Appl. Physiol.* **71**(6), 2469–2475 (1991)
32. Rapoport, S.I.: *Blood-brain barrier in physiology and medicine*. New York : Raven Press, 1976
33. ReKate, H.L., Brodkey, J.A., El-Sakka, W., Ko, W.H.: Ventricular volume regulation: a mathematical model and computer simulation. *Pediatr Neurosci* **14**, 77–84 (1988)
34. Renkin, E.M., Watson, P.D., Sloop, C.H., Joyner, W.M., Curry, F.E.: Transport pathways for fluid and large molecules in microvascular endothelium of the dog's paw. *Microvasc. Res.* **14**, 205–214 (1977)
35. Sorek, S., Bear, J., Karni, Z.: A non-steady compartmental flow model of the cerebrovascular system. *J Biomechanics* **21**, 695–704 (1988)
36. Stevens, S.A.: Mean Pressures and Flows of the Human Intracranial System as Determined by Mathematical Simulations of a Steady-State Infusion Test. *Neurological Research*, **22**, 809–814 (2000)
37. Stevens, S.A., Lakin, W.D., Goetz, W.: A differentiable, periodic function for pulsatile cardiac output Based on heart rate and stroke volume. *Mathematical Biosciences*, 2003 (to appear)
38. Stevens, S.A., Lakin, W.D.: Local Compliance Effects on the Global CSF Pressure-Volume Relationship in Models of Intracranial Pressure Dynamics. *Mathematical and Computer Modelling of Dynamical Systems.* **6**(4) 445–465 (2000)
39. Sullivan, H., Allison, J.: Physiology of cerebrospinal fluid. In: Wilkins R, and Rengachary S, eds. *Neurosurgery* New York: McGraw Hillbook Co. **3**, 2125–2135 (1985)
40. Taylor, A.E., Granger, D.N., Brace, R.A.: Analysis of lymphatic protein flux data. I. Estimation of the reflection coefficient and permeability surface area product for total protein. *Microvasc. Res.* **13**, 297–313 (1977)
41. Tourtellotte, W.W., Shoir, R.J.: Cerebrospinal fluid. In Youmans JR, ed. *Neurological Surgery*. Philadelphia, Saunders, 335–363 (1990)
42. Watenpugh, D.E., Breit, G.A., Ballard, R.E., Zietz, S., Hargens, A.R.: Vascular compliance in the leg is lower than that in the neck of humans. *Medicine and Science in Sports and Exercise* (Suppl. 5):**S26**(137), 1993